Chapter 8: Plasma operation and control

Y. Gribov[1,a], D. Humphreys[2], K. Kajiwara[2], E.A. Lazarus[3], J.B. Lister[4], T. Ozeki[5], A. Portone[6], M. Shimada[1], A.C.C. Sips[7] and J.C. Wesley[2]

ITPA Topical Group on MHD and ITER International and Participants Teams

[1] ITER Organization, Cadarache Centre, 13108 St Paul Lez Durance, France
[2] General Atomics, PO Box 85608, San Diego, CA 92186-5608, USA
[3] Oak Ridge National Laboratory, Oak Ridge, TN 37831-6169, USA
[4] CRPP-EPFL, Station 13, Lausanne 1015, Switzerland
[5] Japan Atomic Energy Agency, Naka-shi, Ibaraki 311-0193, Japan
[6] FDA- Close Support Unit, Garching, Boltzmannstrasse 2, Garching D-85748, Germany
[7] Max-Planck-Institute for Plasma Physics, Boltzmannstrasse 2, Garching D-85748, Germany

E-mail: Yuri.Gribov@iter.org

Abstract

The ITER plasma control system has the same functional scope as the control systems in present tokamaks. These are plasma operation scenario sequencing, plasma basic control (magnetic and kinetic), plasma advanced control (control of RWMs, NTMs, ELMs, error fields, etc) and plasma fast shutdown. This chapter considers only plasma initiation and plasma basic control. This chapter describes the progress achieved in these areas in the tokamak experiments since the ITER Physics Basis (1999 *Nucl. Fusion* **39** 2577) was written and the results of assessment of ITER to provide the plasma initiation and basic control. This assessment was done for the present ITER design (15 MA machine) at a more detailed level than it was done for the ITER design 1998 (21 MA machine) described in the ITER Physics Basis (1999 *Nucl. Fusion* **39** 2577). The experiments on plasma initiation performed in DIII-D and JT-60U, as well as the theoretical studies performed for ITER, have demonstrated that, within specified assumptions on the plasma confinement and the impurity influx, ITER can produce plasma initiation in a low toroidal electric field ($0.3\,\mathrm{V\,m^{-1}}$), if it is assisted by about $2\,\mathrm{MW}$ of ECRF heating. The plasma basic control includes control of the plasma current, position and shape—the plasma magnetic control, as well as control of other plasma global parameters or their profiles—the plasma performance control. The magnetic control is based on more reliable and simpler models of the control objects than those available at present for the plasma kinetic control. Moreover the real time diagnostics used for the magnetic control in many cases are more precise than those used for the kinetic control. Because of these reasons, the plasma magnetic control was developed for modern tokamaks and assessed for ITER better than the kinetic control. However, significant progress has been achieved in the plasma performance control during the last few years. Although the physics basis of plasma operation and control is similar in ITER and present tokamaks, there is a principal qualitative difference. To minimize its cost, ITER has been designed with small margins in many plasma and engineering parameters. These small margins result in a significantly narrower operational space compared with present tokamaks. Furthermore, ITER operation is expensive and component damage resulting from purely operational errors might lead to a high and avoidable repair cost. These factors make it judicious to use validated plasma diagnostics and employ simulators to 'pre-test' the combined ITER operation and control systems. Understanding of how to do this type of pre-test validation is now developed in present day experiments. This research push should provide us with fully functional simulators before the first ITER operation.

PACS numbers: 28.52.−s, 52.55.Fa, 52.55.−s

(Some figures in this article are in colour only in the electronic version)

Contents

1.   Introduction
2.   ITER plasma control system

---

[a] Author to whom any correspondence should be addressed.

1. Introduction

Plasma control is the supreme manifestation of tokamak science and operational know-how documented in [1]. This chapter introduces readers to the current status of plasma operation and means of control, with emphasis on applications of former knowledge and recent results for the ITER design and recent progress to the present ITER design (15 MA) and the proposed operation plan [2]. The science and technology basis of operation and control applicable to ITER has been accumulated in what is now 50 years of development of tokamak and related toroidal magnetic fusion experiments.

A detailed discussion of the underlying science and technology bases (and nomenclature) for plasma control presented here can be found in [1]. All of the considerations described therein continue to be applicable to the present 15 MA ITER design and to the associated operation plan for the physics-phase. This chapter provides an update of new findings and progress topics related to ITER operation and control. Section 2 describes the ITER plasma control system (PCS). Section 3 reviews recent results underpinning the proposed scenario by plasma initiation in ITER, while section 4 discusses 'basic' plasma control.

The discussion of 'basic' plasma control for ITER comprises both magnetic configuration control (e.g. plasma current and equilibrium control, both dynamic and static) familiar from the present tokamak and 'basic' plasma kinetics control. For ITER the latter subject will include static and dynamic control of the fusion power level (burn control) and the provision of means to effect a well-controlled fusion power (burn) start-up and shutdown.

The discussion in section 4 excludes certain aspects of MHD plasma operation control—such as active control of resistive wall modes (RWMs), neoclassical tearing modes (NTMs), sawteeth and edge-localized-modes (ELMs) which are described in chapter 3 of this issue [3]. While these types of control are described in chapter 3 [3] as being 'advanced', NTM and ELM control are presently projected to be required for sustained fusion burn operation in the 'basic' ITER ELMy H-mode reference scenario. In this sense, these aspects of 'advanced' MHD control will likely be a routine part of 'basic' ITER plasma control and will undoubtedly be effected via the same ITER PCS (described in section 2) that will be responsible for 'basic' plasma operation scenario implementation and plasma operation control.

Active RWM control effected by magnetic means (feedback control using external non-axisymmetric fields) plus at least some degree of active current profile control and some degree of 'active' control of internal transport barrier (ITB) characteristics are currently expected to be required for ITER long-pulse (proto-steady-state) operation in a reversed-shear 'advanced scenario'. Progress and projections for ITER in this still-evolving area of tokamak science and R&D are addressed in chapter 6 of this issue [4].

The discussion of 'basic' plasma control status also addresses the related subject of how control and monitoring of plasma operation participate in the protection of ITER systems against the normal and the abnormal effects of plasma operation. This aspect of plasma control—already of some importance in present tokamaks—assumes a higher level of importance for reactor tokamaks and ITER because the plasma energies and surface energy deposition levels inherent in reactor-regime operation have a higher potential to effect surface damage to plasma facing components. Hence, the need for comprehensive protection of reactor tokamak systems against damage produced by plasma operation is arguably higher—for both economic and safety reasons—than in present tokamaks. The desire to predict the effects of plasma operation on the ITER plant systems also gives rise to the final subject of section 4: the need for development of a comprehensive plasma operation and control simulator that can be used for pre-operation planning and optimization of ITER plasma operation procedures, experimental plans and plasma scenarios.
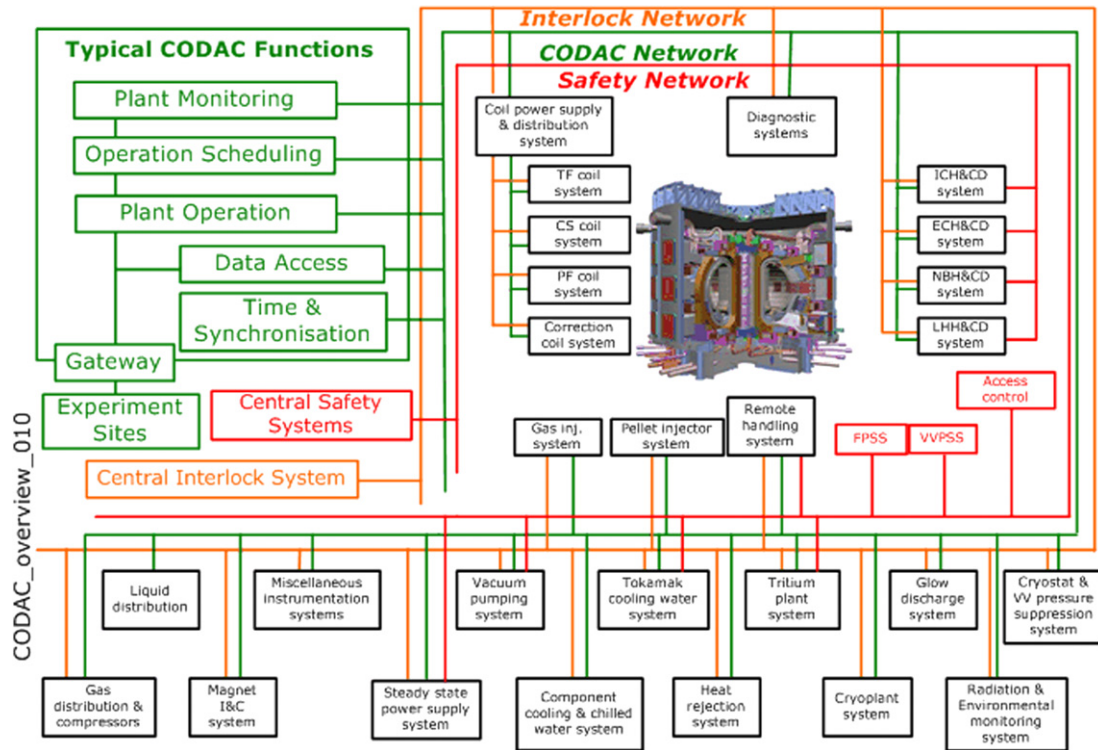
Figure 1. Simplified scheme of the ITER plant control system.

2. ITER plasma control system

ITER will have all the main systems essential to control plasma operation in future fusion power plants. A simplified scheme of the ITER plant control system is shown in figure 1. The plant will be controlled by three independent systems [2]: in normal operation by the control data access and communication (CODAC) system and in some types of off-normal operations by the central interlock system (CIS) and central safety systems (CSS). CODAC provides high level command to systems dedicated to the control and the operation of each part of the complex ITER plant, general software functions for the benefit of these systems, synchronization for these systems, high bandwidth backbone communication networks, coordination of data logging and the processing of data from the plant systems, as well as management of the experimental databases. The CIS, independently of CODAC, ensures plant-wide protection of investment, in case of off-normal events. The safety systems provide fusion and plasma termination, when it is required for safety or personnel protection.

The ITER plasma control system has the same functional requirements as the control systems in present tokamaks [1]. These are plasma operation scenario sequencing, basic magnetic control, basic kinetic control, advanced plasma control and plasma fast shutdown. The plasma operation scenario sequencing is a choice of sequence logic, as well as command signals and target waveforms for the individual plant system controllers. The basic magnetic control includes control of plasma initiation, control of plasma current, position and shape, as well as correction of error fields. The control is provided by the central solenoid (CS), the poloidal field (PF) coils and the error field correction coils. The basic kinetic

control includes control of basic plasma parameters other than current, position and shape. The control is provided by the fuelling and the exhaust systems in combination with heating and current drive systems. The advanced plasma control includes feedback control with the goal of improving plasma performance, e.g. control of RWMs, NTMs, sawteeth, ELMs and ITB. Both magnetic and kinetic actuators are used in this type of control. The plasma fast shutdown is a discharge termination system used when it is impossible to provide shutdown in a normal controlled way. The goal is to mitigate damaging effects on the machine from unavoidable disruptions (heat and mechanical loads, runaway electrons). An example of a tool for the fast plasma shutdown is the massive injection of a noble gas such as neon.

3. Plasma initiation

Plasma initiation in ITER and similar future reactor tokamaks will have to be effected with an in-vessel toroidal electric field, E_{T}, that will be $\leqslant 0.3 \,\mathrm{V\,m^{-1}}$. This limitation on E_{T} arises owing to the use of superconducting poloidal field coils. In addition, ITER and many proposed future tokamaks incorporate toroidally continuous vacuum vessels and/or in-vessel structures that will generate appreciable in-vessel poloidal 'stray' fields (axisymmetric poloidal fields normal to the toroidal field B_{T}), denoted herein as $B_{\perp}$, that impede plasma initiation by a Townsend avalanche in a low-pressure fill gas. The theory of Townsend avalanche initiation in a tokamak with finite stray fields and its application to the start-up of the 'ITER-Design 1998' (21 MA plasma current, 8.14 m major radius, 2.8 m minor radius, monolithic central solenoid) is treated in [1]. As per the theory, the minimum

Table 1. Minimum toroidal electric field for Townsend avalanche breakdown.

E_{min} (V m^{-1})	L (m)	p (mPa)	$E_{min} \times L$ (V)
0.334	200	3.29	67
0.133	500	1.44	67
0.067	1000	0.66	67
0.033	2000	0.33	67

toroidal electric field, E_{min}, for avalanche growth in room-temperature (300 K) H_2 or D_2 or T_2 gas at pressure p(Pa), for a free-streaming-electron connection length, L(m), is given by

$$E_{min} = 950p/\ln(3.88pL) \text{ V m}^{-1}. \quad (1)$$

Equation (1) and various supporting experimental data are plotted in figure 12 of [1]. Table 1 summarizes E_{min} data calculated using equation (1) for a range of L and p values relevant to present tokamaks and ITER.

For reliable breakdown, $E \geqslant 2E_{min}$ is desirable [5]. For ITER at 0.3 V m^{-1}, $p = 1.4$ mPa ($\approx 1.1 \times 10^{-5}$ Torr) and $L = 500$ m is predicted to yield reliable 'Ohmic' (without EC-assist) Townsend avalanche breakdown.

Table 1 demonstrates that $E_{min} \times L$ is a constant, independent of p: for marginal avalanche growth, an average free-streaming electron must gain about 70 eV before it interacts with the fill gas or is lost to the torus wall. This energy gain criterion means that the voltage gain between torus wall interactions ($E \times L$) rather than E_T or $E_T B_T/B_\perp$ is the parameter that most directly determines whether or not the avalanche grows. Data presented in section 3.1.1 explicitly confirm this premise.

The magnitude of the stray fields determine the value of L. As per [1, section 2.3.1, equation (3)], which in turn is based upon the considerations given in [6], the recommended basis for estimating the 'effective' (Lloyd) connection length is $L_{eff} = 0.25a_{eff}B_T/B_\perp$, where B_T is the toroidal field at the major radius, R_{null}, of the multipole field-null region where breakdown is expected to occur, a_{eff} is the minor radius of the null region and $B_\perp$ is the poloidal stray field magnitude at the null-region boundary. In [6], it is not explicitly specified how one averages $B_\perp$ around the null-region boundary: in the cases where the contours of $|B_\perp|$ vary significantly around the null-boundary circle, common practice has been to take a null-region boundary circumference-weighted average to arrive at an effective value of $B_\perp$. Examples of the application of this type of boundary-average criterion to the start-up for the 'ITER-Design 1998' are given in [1]. The conclusions reached therein were that while the null size and the quality sufficient to assure reliable Ohmic breakdown at 0.3 V m^{-1} should be possible, it would be desirable to provide electron cyclotron (EC) assist to improve avalanche growth reliability and/or relax null quality requirements and also to provide plasma initiation energy balance assist during the impurity ionization ('burn-through') phase that follows Townsend breakdown.

3.1. Plasma initiation in present tokamaks

A comprehensive study of Ohmic and EC-assisted plasma initiation was done in DIII-D in the early 1990s [6]. Some of the results reported therein are revisited in a later paper on DIII-D plasma initiation [7] with improved-null control
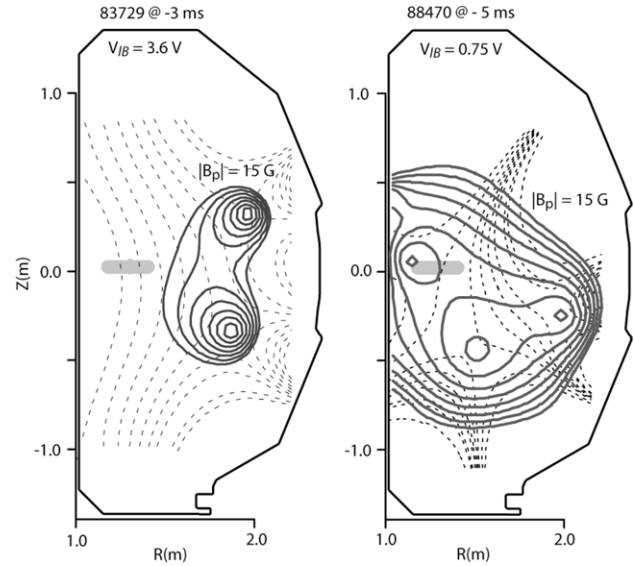
Figure 2. Field-null poloidal flux (- - - -) and field magnitude contours (——) for DIII-D plasma initiation with previous (#83729) and feedback-optimized poloidal field system control (#88470). The vessel-surface voltage, V_{IB}, at which initiation occurs is indicated. The shaded in-vessel region indicates the major radius where the plasma breakdown is observed to develop. Compiled from data in [7].

and wall conditioning. Recent work on ECH-assisted plasma initiation is now reported for JT-60U [8]. Earlier work with EC-assist on smaller devices is summarized in [9]. A full description of the atomic physics during the avalanche and the ionization phases is contained in [10]. The basis for the application of equation (1) to predict tokamak plasma initiation and to interpret initiation data is well detailed in [6] and is also summarized in [1]. The presentation that follows in sections 3.1.1 and 3.1.2, respectively, reprises past and new (after the ITER Physics Basis) data on Ohmic and EC-assisted initiation. Section 3.1.3 summarizes the overall findings from the new data.

3.1.1. Ohmic discharge initiation. Results [7] obtained after the writing of [1] supplement the conclusions about ITER initiation reported therein. The data and analysis presented in [7] detail Ohmic breakdown and current initiation (impurity burn-though) observations obtained in DIII-D after changes made in the Ohmic heating coil and the power system mandated revision of the plasma initiation control procedures used for the previous DIII-D studies reported by [6]. For the new procedure, a closed loop feedback control algorithm that takes induced vacuum vessel currents into account was implemented to automatically achieve optimal in-vessel null quality at the time of initial breakdown. Figure 2 shows the EFIT-reconstructed null configurations obtained with the previous (Lloyd *et al* [6]) and the improved (Lazarus *et al* [7]) magnetic control schemes. The improvement in the null quality and the corresponding reduction in the externally measured vessel-surface loop voltage, V_{IB}, at the time of initiation (first H_α light) is evident.

The data in figure 3 demonstrate that in DIII-D, the major radius at which plasma initiation (Townsend avalanche and initial current channel formation) first develops lies at or
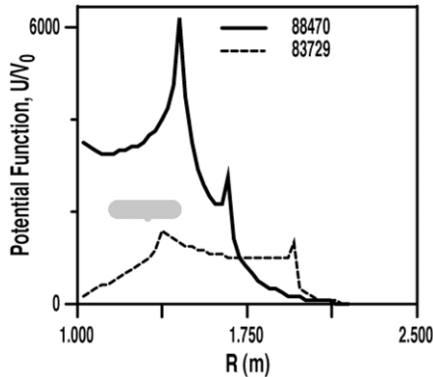
Figure 3. Surface-voltage-normalized potential, U/V_o, for the DIII-D examples shown in figure 2. The shaded region indicates the major radius range, determined from H_α light observations, for initial breakdown in both examples.

near the major radius where the field-line-following potential function $U(R) \equiv \int_{\text{along} B} dl\, V_{IB}$ is maximum. This line integral is evaluated numerically, from equilibrium reconstruction data, for a set (grid) of possible starting locations (R, z), until the field line reaches the vessel wall. For the outside-null example (#83729), initiation is observed to occur at a major radius $R = 1.3$ m, whereas the null is centred at $R = 1.8$ m. A similar but smaller inboard shift of the breakdown R relative to the null R is observed for the improved-null example. In both cases, the breakdown location data confirms the hypothesis that voltage gain ($\int E_T\, dl$) along the free-streaming field lines, rather than E_T at the null centre or $E_T B_T/B_\perp$ at the null centre/edge, is the most direct arbiter of where breakdown initially develops. The field-line-following estimate of the maximum connection length for #88470 is $L_{\max} \approx 4.5$ km. This value applies for the field line starting at $R = 1.3$ m. The average connection length for starting points near the null centre ($R \approx 1.8$ m) is about 1.5 km. For $E_T = 0.09$ V m^{-1}, the corresponding estimated free-drift voltage gains are about 405 V (#88470) and 135 V (#83729) (compared with 67 V from equation (1) and table 1).

For the improved-null example shown, the measured vessel-surface voltage V_{IB} at which initial breakdown occurs was about 0.75 V, with a corresponding estimated in-vessel $E_T \approx 0.09$ V m^{-1} (compared with $V_{IB} = 3.6$ V and $E_T \approx 0.32$ V m^{-1} for #83729). The improved null quality that the new feedback control scheme provides is also evidenced by the ability to obtain plasma initiation at B_T values as low as 0.34 T, whereas the previous lower B_T limit was 0.6 T.

The reconstruction-derived null-region centre and $R = 1.3$ m connection lengths for #83729 are, respectively, about 1.4 and 1.2 km. At 0.32 V m^{-1}, the free-drift voltage gains are about 448 and 384 V. In both examples, the estimated free-drift voltage gains equal or exceed the ≈ 130 V threshold predicted to be needed for reliable avalanche initiation.

The observations cited above show the benefit of improved-null quality (reduced stray field). However, plasma operation experience with the improved control scheme also showed that variation in loop voltage at initial breakdown, V_{IB}, is also correlated with the initial carbon concentration (as evidenced by CIII spectroscopic data), which is in turn correlated with machine conditioning and usage [7]. The lowest breakdown voltage observed in Ohmic plasmas is

0.75 V, corresponding to $E_T \approx 0.09$ V m^{-1}. However, at-breakdown E-fields are more typically 0.25–0.5 V m^{-1}, and attainment of lower at-breakdown E-fields is not strictly controllable by null quality alone. The authors of [7] surmise that wall conditions contribute to determining the at-breakdown E-field: if the vessel conditions are 'pristine', with a hard carbon surface, the lower range of at-breakdown values are obtained; however, if the experiments involve, for example, heavy gas puffing, which tends to make the carbon surface sooty, the values will be at the higher end of the range.

The 1998 DIII-D results can be compared with the earlier JET [9] work, which reported reliable breakdown at $E_T B_T/B_\perp > 1000$ V m^{-1}. The DIII-D results at $B_T = 2.1$ T are typically $1500 < E_T B_T/B_\perp$ (V m^{-1}) < 3000. Values as low as $E_T B_T/B_\perp \approx 850$ V m^{-1} have been achieved. Given that there is nearly a factor of two difference in the major radii between DIII-D and JET, the two sets of $E_T B_T/B_\perp$ criteria are in good agreement with each other and with Townsend theory embodied in equation (1). We also conclude here that the $E \times L$ estimates of free-drift voltage gain for the DIII-D start-up are in similarly good agreement with Townsend theory and that the method can be applied to evaluate Townsend avalanche characteristics and breakdown localization for ITER. This evaluation is treated explicitly in section 3.2.

3.1.2. ECH-assisted discharge initiation. Studies of electron-cyclotron-assisted plasma initiation in various tokamaks (see [9] and references cited in [8]) have confirmed that EC-assist facilitates reliable initiation at low E_T and/or with higher-than-optimal stray fields. With 700 kW of 60 GHz fundamental ECH assist power, breakdown in DIII-D could be obtained at $E_T \geqslant 0.15$ V m^{-1}, whereas $E_T \geqslant 0.25$ V m^{-1} was required for otherwise similar parameters for Ohmic startup [6]. The latter estimate for Ohmic-start-up E_T is obtained under the assumption made in [6] that the breakdown occurred at the vessel geometric centre. Since the evidence given in [7] suggests it is likely that the breakdown occurred at a somewhat smaller radius, the Ohmic-minimum value likely remains as $E_T = 0.3$ V m^{-1}. The corresponding EC-assisted vessel-surface loop voltage value, $V_{IB} = 1.9$ V, as reported in [6], can be directly compared with the Ohmic-startup surface loop voltage reported in [7] where $V_{IB} \approx 2$ V is routinely obtainable with a well-conditioned vessel. One may say that with optimal null quality (low stray field) and wall conditioning, the incremental benefit of EC-assist in further reducing the minimum breakdown voltage is modest.

In [6], Ohmic- and EC-assisted cases are reported wherein a large radial stray field was deliberately introduced. Here the advantage of the EC-assist in producing breakdown was very clear. With $L \approx 0.35$ km, $E_T B_T/B_\perp \approx 280$ was obtained. At the next highest stray-field setting, with $L \approx 0.28$ km, there was breakdown, but the current channel did not sustain. In comparing the Ohmic- and the EC-assisted cases under high stray field conditions, the threefold increase in $E_T B_T/B_\perp$ is quite dramatic. However, since the failure in the Ohmic example is in the buildup of the current channel, the comparison between the Ohmic- and the EC-assist is more complex than simply the effect of EC on the breakdown condition.
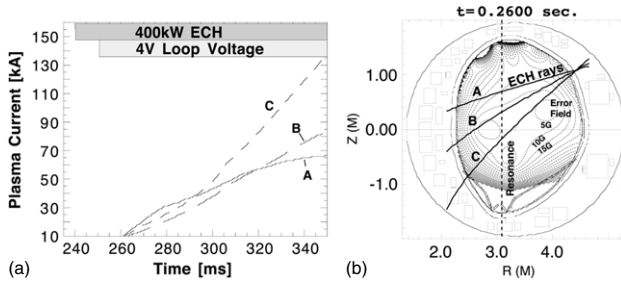
Figure 4. Dependence of plasma current ramp-up in ECH-assisted discharges in JT-60U [8]: (*a*) Time evolution of plasma current, (*b*) ECH resonance position (shown as an intersection of the rays with the resonance major radius position). The ray-labels A, B and C correspond to the waveforms labelled 'A, B, C' in (*a*). The error fields are also displayed in (*b*).

In Ohmic plasma initiation experiments on JT-60U [11] which were reported in [1], the null conditions were quite good and low loop voltage plasmas with $E_T = 0.08\,\mathrm{V\,m^{-1}}$ could be obtained with helium pre-fill gas and the assistance of 1.5 MW of lower hybrid range of frequencies (LHRF) heating. Recent EC-assisted start-up experiments in JT-60U with an 'ITER-like' EC system (with up to 950 kW of fundamental 110 GHz EC power (93% O-mode[8])) launched from the low-field side clearly demonstrate the beneficial effects of EC-assist [8]. The experiments focused on the effects of pre-fill pressure, polarization and location of the resonant region relative to the null location.

With a radially centred fundamental resonance and the standard JT-60U null configuration, the breakdown voltage in H_2 was reduced with 400 kW of power from 30 to 4 V. The corresponding estimated at-breakdown electric field is $E_T \approx 0.26\,\mathrm{V\,m^{-1}}$, with $E_T B_T / B_\perp \approx 800$. The EC power could be decreased to 200 kW without a significant increase in the breakdown voltage or degradation of the initial I_p ramp-up rate. A study of H_2 pre-fill pressure and EC polarization, launch angle and resonance position was performed with $E_T = 0.26\,\mathrm{V\,m^{-1}}$ and 400 kW EC input. The pre-fill scan showed an approximately linear relation between the initial plasma density, n_{el} (tangential line density, measured 25 ms after ECH injection), and the pre-fill pressure, p_o, which is represented by $n_{el}[\mathrm{m^{-2}}] = 1.65 \times 10^{18} p_o$ [mPa] (the p_o range is 2.7–6.7 mPa). The I_p ramp-up rate decreases when the pre-fill pressure is increased to 1.6 mPa. Changing to the X-mode[9] dominant EC injection (43% O-mode) also results in the degradation of the I_p ramp-up rate.

The initial density of the X-mode assisted discharge is the same as the O-mode dominant discharge; nevertheless, the X-mode component is reflected as soon as the plasma density is increased. The rest of the ECH power (O-mode component) is not enough for a robust I_p ramp-up. Varying the EC injection angle (which changes in the flux surface location of the resonance) also affects the I_p ramp-up rate (figure 4). Careful adjustment of the location of the EC resonance layer in relation to the field null gives optimal (highest dI_p/dt) plasma

---

[8] The O mode resonance occurs for a linearly polarized wave travelling perpendicular to the magnetic field with the electric field parallel to the magnetic field.

[9] The X mode resonance occurs for a circularly polarized wave travelling along the magnetic field.

initiation. Successful second-harmonic EC-assisted start-up was also achieved with 950 kW of O-mode power. However, an attempt to obtain a third-harmonic start-up with 1600 kW of O-mode power produced only a weak initial breakdown without subsequent plasma current sustenance and ramp-up.

The JT-60U observations clearly demonstrate that the EC injection angle affects many parameters applicable to start-up, such as initial plasma location, ECH absorption, gas recycling and initial plasma impurity content. The distinction between the EC-assist of Townsend breakdown (seen for a wide range of EC and gas-fill parameters) and the current sustenance and ramp-up (seen only for a more limited range of pressure and with properly positioned first- and/or second-harmonic resonances) is also demonstrated in [8]. In addition, second-harmonic assist with a resonance positioned near the inboard limiter is found to be possible, but requires a four-fold increase in input power.

3.1.3. Summary. Plasma initiation studies reported since the compilation of the ITER Physics Basis confirm the 'effective connection length' interpretation of Townsend avalanche theory as recommended in [1, 6] and clearly demonstrate the importance of providing both adequate field-null quality and also well-conditioned torus walls. The field-line-following analysis described in [7] for optimized DIII-D Ohmic start-up confirms the significance of $E_T \times L \geqslant 130\,\mathrm{V}$ as the fundamental criterion for robust Townsend avalanche growth and provides a new methodology for evaluating ITER Townsend breakdown characteristics. Electron-cyclotron-assisted start-up experiments conducted in JT-60U with first-harmonic absorbed powers in the 200–400 kW range clearly demonstrate the importance of the co-location of the resonance and the field-null regions and confirm, in general, the ITER-proposed strategy for providing several MW of first-harmonic EC start-up assist. The feasibility of using a second-harmonic assist, albeit with a need for increased EC power, is also demonstrated.

3.2. Plasma initiation in ITER

The application of the Townsend avalanche, field-null quality and EC-assist for breakdown and current ramp-up considerations noted above for the 'ITER-Design 1998' design was presented in the ITER Physics Basis [1]. The work summarized below followed up the application of the same considerations to the present ITER design (15 MA, 6.2 m major radius, 2 m minor radius, segmented central solenoid). The application of the field-line-following criterion for avalanche growth and simulation of EC-assist energetics during the impurity 'burn-through' phase of start-up has also been completed. The results of these studies confirm the feasibility of achieving robust Ohmic Townsend breakdown and EC-assisted impurity burn-through and current ramp-up.

Because of the difficulty in cooling and the precise alignment of the plasma facing components located near the central solenoid, only outboard or almost central plasma initiation are adopted for ITER. In both cases, during the limiter phase, the plasma contacts two actively cooled limiters located in opposite equatorial ports. In inductive scenarios with full current, for reduction of the resistive flux losses, the plasma
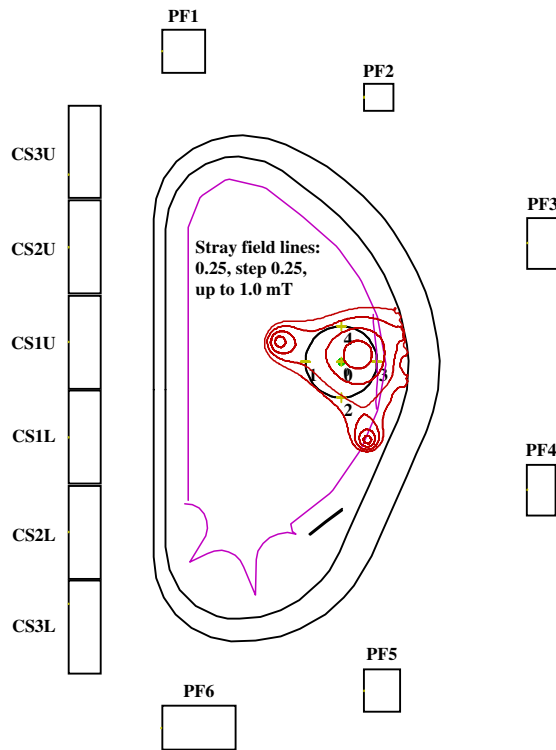
Figure 5. The ITER CS and PF coils, the vacuum vessel and blanket support (black lines), the plasma facing line of the first wall, limiter and divertor (magenta line), the breakdown region (black circle) and the lines of constant residual magnetic field at the breakdown ($t = 0.85$ s): 0.25, 0.5, 0.75, 1.0 mT (red lines).

Figure 6. (*a*) Plasma current versus time; (*b*) vertical and horizontal magnetic fields in the five points of the breakdown region (shown in figure 5) versus time.

start-up will be provided with the plasma minor radius growing consistently with the increase in the plasma current (keeping the value of q on the plasma boundary approximately constant). For simulations of these scenarios plasma initiation is assumed to start from the region distant by about 0.8 m from the limiter. For steady state or hybrid scenarios with lower plasma current (<13 MA) almost central plasma initiation can be performed. This start-up reduces the rate of reduction of the value of q in the plasma centre. In these scenarios, simulations of plasma initiation were performed assuming the plasma centre distant from the limiter by about 1.6 m.

The studies of ITER plasma start-up have taken the detailed 'engineering design' characteristics of the poloidal field (PF) coil system and the power supplies into account. The PF coil system comprises a segmented central solenoid (CS) and six outer PF coils, as shown in figure 5. All PF coils and all CS modules, except for the two central modules, have independent power supplies. The two central CS modules are connected in series in a common circuit. The reference case 15 MA plasma scenario starts with a fully magnetized CS. At the start of the CS discharge, the fully magnetized PF system produces about 120 Wb of flux in the breakdown region (circular area: $R = 7.48$ m, $Z = 0.62$ m, $a = 0.8$ m). With full magnetization, the nominal in-vessel toroidal electric field at the centre of the breakdown region is $E_T = 0.3$ V. Approximately 2 MW of the 127 GHz ECH 'start-up' assist will be provided to increase reliability of the plasma initiation and support impurity 'burn-through' in the initial current ramp-up phase.
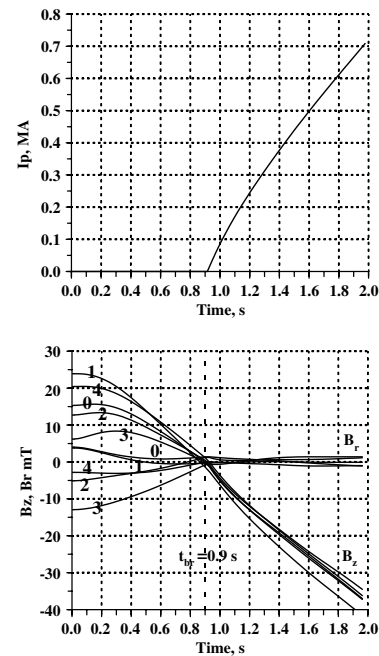
The ITER torus vacuum vessel (shown schematically in figure 5) has a toroidal resistance of 7.7 $\mu\Omega$ and the initial CS discharge drives about 2 MA of toroidal eddy currents at breakdown. These eddy currents delay the breakdown by about 0.9 s after the start of the CS discharge and result in a before-breakdown loss of about 9 Wb of an initial magnetization flux.

Studies of plasma initiation in ITER are performed by simulations, which take into account eddy currents in the conducting structures and models of the power supplies (in particular, the set of resistors in the PF power supply switching networks). Several codes were used in these studies: the 2D electromagnetic code TRANSMAK [13] comprising the 0D transport code SCENPLINT and the 3D electromagnetic code BDOS [14]. The studies have shown the capability of the PF system to provide outboard or almost central plasma initiation, starting from 45% to 100% of the maximum CS magnetization. It should be noted that the PF system can also support the inboard plasma initiation. However, the required precise alignment of the plasma facing components located near the central solenoid and their active cooling seems impossible.

Results of simulation of plasma initiation in inductive scenarios, performed with the code TRANSMAK, are shown in figures 5 and 6 [15]. In this example, the discharge starts from a fully magnetized CS, which produces 123 Wb of magnetic flux in the breakdown region (the circle in figure 5). At 0.85 s, when 2 MW of EC power is applied, E_T in the breakdown region reaches 0.3 V m^{-1}, and the $B_\perp$ residual field inside the breakdown region drops to $\leqslant$1 mT (the toroidal magnetic field, B_T, at the null centre is 4.4 T). The contours of constant $B_\perp$ at $t = 0.85$ s are shown in figure 5. The effective 'Lloyd' connection length, $L_{eff} = 0.25a_{eff}B_T/B_\perp$, as recommended in [1] is about 1.7 km; the maximum connection length evaluated using the field-line-following method described in [7] is about 18 km (when averaged over

25×25 cm meshes). The voltage gains at $0.3 \, \text{V m}^{-1}$ for an 'average' or a 'maximum-gain' free-streaming electron are, respectively, about 500 V and 5500 V. By either interpretation of Townsend avalanche theory, robust breakdown over a rather wide range of gas pressures: from 0.3 mPa (2.3×10^{-6} Torr) to 10 mPa (7.5×10^{-5} Torr), is expected. Considerations of runaway electron avoidance during the start-up increase the usable lower pressure bound to about 0.5 mPa (3.8×10^{-6} Torr). The magnetization flux obtained at breakdown is 114.6 Wb.

After breakdown, the impurity burn-through and the evolution of the plasma density and temperature were simulated with the 0D transport code SCENPLINT, which is incorporated within the TRANSMAK code. The operational range of gas pressure, limited by impurity burn-through, is narrower than that limited by the Townsend avalanche breakdown. In the simulation, the impurities are C and Be and their concentration increases with a time constant of 0.25 s until concentrations of 4.3% and 2% are reached, respectively:

$$\frac{n_{\text{C}}}{n_{\text{e}}} = 0.013 + 0.03[1 - \exp(-t/\tau)],$$

$$\frac{n_{\text{Be}}}{n_{\text{e}}} = 0.02[1 - \exp(-t/\tau)], \qquad \tau = 0.25 \, \text{s}. \qquad (2)$$

The transport model takes into account recombination, ionization and charge-exchange of all ionization states of the impurities [16]. Other assumptions used in the simulation are as follows. The gas pressure is 0.8 mPa (6×10^{-6} Torr) and the EC power is 2 MW. The plasma energy confinement time is taken to be the maximum of the times calculated using the Bohm confinement scaling $3 \times 10^{-3} a^2 B_{\text{t}} T_{\text{e}}$ [s, m, T, keV] or the ITER-98 L-mode confinement scaling [17].

With the maximum toroidal electrical field produced by the PF system (about $0.3 \, \text{V m}^{-1}$), the plasma current increases with the rate of $0.68 \, \text{MA s}^{-1}$, as is shown in figure 6(*a*). The vertical and the horizontal components of the magnetic field at the five points on or within the breakdown region are given in figure 6(*b*) (the numbering of the points is shown in figure 5). When the plasma current increases, this magnetic field ensures plasma equilibrium in the breakdown region. The equilibrium is stable: the decay index of the vertical magnetic field, defined as $n = -R/\langle B_z \rangle \cdot \text{d}\langle B_z \rangle / \text{d}R$, where $\langle B_z \rangle$ is the vertical magnetic field averaged over the breakdown region, is close to 0.5. During 1 s after breakdown, the plasma density increases to $0.6 \times 10^{19} \, \text{m}^{-3}$, the temperatures of electrons and ions increase to 0.8 keV and 0.3 keV, respectively, and the value of Z_{eff} increases to 2.3. The coil currents, voltages and the total active power during plasma initiation, as well as the magnetic fields and the forces on the coils, are all within design limits.

The additional studies performed with the TRANSMAK code show that the cryostat, the conducting structures located outside the cryostat and the vacuum vessel ferromagnetic inserts have only a minor magnetic effect on the plasma initiation scenario.

The effect of 3D eddy currents induced in the vacuum vessel was studied with the code BDOS. The presence of ports and the perturbation to the overall axisymmetric eddy current flow that their presence introduces causes a deterioration, for otherwise fixed PF coil programming, in the field-null quantity obtained in the above-cited axisymmetric calculations without ports. At breakdown, the stray magnetic field, averaged over the toroidal direction, in the breakdown region increases by a factor of 2 to 3. However, this deterioration can be mitigated. It was shown that it is possible to significantly reduce the deterioration of the field null by re-optimizing the resistance in the switching network to apply voltages that minimize breakdown region residual fields with the axisymmetric effect of the ports taken into consideration. We note, however, that even without re-optimization, the null quantity obtained in our 'open-loop' 3D calculation is still adequate to assure Ohmic breakdown.

In summary, detailed magnetic and plasma energy balance simulations of EC-assisted plasma initiation in ITER, done with engineering design models of the PF coil, vessel and PF power systems, show that successful Townsend avalanche initiation and current ramp-up on the outboard limiter can be expected. The plasma energy balance studies suggest, subject to the usual physics data qualifications about uncertainties in modelling the energy balance and the impurity influx dynamics of plasma start-up, that the planned provision of 2 MW of first-harmonic EC start-up assist is both prudent and adequate.

4. Basic plasma control

4.1. Magnetic position and configuration control

4.1.1. Magnetic control in present tokamaks. Magnetic control of shaped tokamaks depends on three challenges: identification of the existing equilibrium, stabilization of the unstable vertical position and regulation of the equilibrium to be as close as possible to the reference equilibrium. Although all three aspects of magnetic control were already highly developed in the previous ITER Physics Basis report [1], most tokamaks continue to develop the associated tools to provide increased precision of the equilibrium as experiments aimed at optimizing the plasma performance themselves become more demanding.

The range of equilibria explored by different devices has increased somewhat, in spite of the coil current limitations on the PF coils on each tokamak. TCV increased its elongation to 2.8, a record for conventional aspect ratios [18]. JET has explored higher triangularity to exploit its effect on high performance. ASDEX Upgrade has developed equilibria with an upper null inside the vessel, although not yet with the up–down symmetry properties of an ideal double-null plasma.

DIII-D has implemented real time equilibrium reconstruction which has allowed great flexibility in changing plasma shapes [19]. As a result, they are in a position to choose between the X-point position control and the strike-point position control for control of the divertor region. The accuracy of the shape identification allows the very small shifts in position (of the order of 1 cm) which are required for neoclassical tearing mode control [20]. The recently upgraded control system, speeded up by about a factor of 20–30 [21], can provide error values to the shape controller at about 4 kHz. Real time estimation of the *q*-profile has also been implemented with a cycle time of 6 ms on a separate real time computer that combines magnetic and motional stark effect data.

On JET, the approach adopted to perform the shape identification is different from the one used in DIII-D. Instead of using an equilibrium code to locate the plasma boundary, the

plasma boundary reconstruction code XLOC [22, 23] uses the available magnetic measurements and the active coil currents to extrapolate the flux in the vacuum, to search for the X-point location and to reconstruct the plasma shape. The calculation has a cycle time in the range of few hundred microseconds. In the area near the X-point, where the spatial flux variation is not monotonic, a more accurate description is used to locate the strike points. This again allows the possibility of identifying and controlling the lower part of the magnetic separatrix instead of the real boundary. In addition, the calculation of the flux expansion and the strike line angles permits the computation of the power loads on the divertor tiles. The precision of the plasma boundary position is within 1 cm at the machine mid-plane and up to 4 cm at the machine top.

On JT-60U the reproduction of the plasma shape is now routinely based on the Cauchy-condition surface method [24, 25], including a scheme for dealing with eddy currents [26] and additionally being used for an estimate of the plasma current profile [27].

Most tokamaks separate the vertical position and the shape control, in view of the different timescales and because most have a separate fast power supply. The position regulators are almost all in the proportional-integral derivative (PID) class, with the exception of JET, which uses modulated on–off step function control of the vertical speed [28], which is inapplicable to ITER. In order to adapt to a wide variation of growth rates and to avoid excessive switching in the amplifiers, the controller gains are varied dynamically to maintain an average switching frequency.

ELMs can have a negative effect on the feedback of the vertical position. Firstly, the loss of plasma energy displaces the equilibrium vertically in an up–down asymmetric configuration and, secondly, the ELM perturbation itself can falsify the measurement of the vertical position, leading to an excessive and non-stabilizing voltage demand on the power supply. The pollution of the estimator of the vertical position by an ELM was investigated statistically and experimentally on TCV and modelled for JET, demonstrating the existence of an improved control resilient to ELMs [29]. The new plasma control on JET will allow the implementation of this approach. A new estimator of the centroid vertical velocity has been implemented on JET combining magnetic measurements taken at four different toroidal positions to reject $n = 2$ components, which also helps clean up the estimator during ELM perturbations [30].

While experiments with different plasma shapes were investigated on ASDEX Upgrade, the occurrence rate of badly damped and sometimes even unstable oscillations of the plasma position dramatically increased, attributed to an increased sampling rate of the digital plasma position controller. The controller gains were based on the assumption of a quasi-continuous controller. New controller gains now respect the actual discrete sampling and have eliminated most of the oscillations. Oscillations with frequencies of 30 Hz still occur in shapes close to double-null configuration. Mechanical torque oscillations of the flywheel generator are small and can only be detected by a special torque measurement system. Unfortunately, the mechanical resonance frequencies of the shafts at 23 and 25 Hz are within the frequency response bandwidth of the feedback loops [31]. To solve this problem

without deteriorating the plasma control, feedback-controlled active damping circuits based on the measured torque modulation of the generator shafts have been installed [32].

We now turn to shape control. Feedback control of the DIII-D discharge shape still uses the isoflux algorithm with a hand-crafted PID controller which is dominantly diagonal. Development of a model-based, multiple-input, multiple-output (MIMO) shape controller is well underway. TCV still uses a model-based MIMO PID controller with no hand-crafting. On the ASDEX Upgrade, the control algorithms are decoupling proportional-integral matrix controllers whose gains are derived from the modelled frequency response of the controlled system. Gains are computed so that the closed loop frequency response is approximated to the response of a reference system. The design method features a load balancing component which allows the use of more coils than control parameters in order to avoid running into coil current limits. A new model-based plasma current and shape controller (XSC, eXtreme Shape Controller) has been developed on JET [33, 34, 35] to improve the control performance with higher elongation and triangularity. The design uses a linearized equilibrium response model [36]. A novel feature is that the number of parameters to be controlled is larger than the number of control inputs to the plant using a singular value analysis to identify the principal directions of the mapping between coil currents and geometrical descriptors. These 'principal directions' are taken as controller outputs. The controller minimizes the difference between the plasma boundary and the desired shape described as a large set of coordinates. In this sense, XSC no longer has one reference waveform for each controlled gap.

From the above brief description of the work on shape control, we can conclude that digital systems are allowing more advanced controllers to be implemented. Teething troubles linked to the digital system latency are evident, but will not present any difficulties to the slower ITER control. However, the number of possibilities for optimally controlling an equilibrium remains large, with little convergence between devices. The underlying reason for this is that the basic weaknesses of all tokamak control systems are linked to their construction details including coil positions, numbers, current and voltage limits, bandwidth and the available diagnostics, rather than the algorithmic approach to the control of the shape for which many solutions have been shown to provide adequate functionality. It is clear that modelling of the full equilibrium control problem is playing a greater role in developing feedback systems. The approaches used range from simple linear models with rigid displacement of the equilibrium, linearized deformable equilibrium models, fully non-linear models with assumed flux conservation through to complete modelling of the tokamak including poloidal flux diffusion and energy transport.

On DIII-D, JET, JT-60U, ASDEX Upgrade and TCV, linear and non-linear plasma models have been developed and tested, including details of the power supply systems. Validating of these different models has continued on many tokamaks and we can only present a rapid survey of these activities.

An upgraded version of the CREATE-L model [5] has been developed specifically for JET, including an equivalent

axisymmetric model of the iron core, a new definition for plasma poloidal beta and a new parametrization of the current density profile [36]. This model has been validated on a set of JET pulses with no plasma, during VDEs and in closed loop simulations. This modelling has led to a deeper understanding of specific experiments, particularly the detection of the neutral point for density limit disruptions [37] and the sudden jump of strike points during ELMs [38]. The plasma jumps due to ELMs were previously reported in [39, 40].

The RZIP rigid displacement model was successfully validated on the JT-60U tokamak for higher temperature plasmas using model estimate techniques developed on TCV [41]. New methods for *a posteriori* adjusting the parametric model were explored using the JT-60U data although it was not possible to improve the dynamical shape control significantly, compared with the tuned feedback [42]. The RZIP model was also used to investigate the control properties of spherical tokamak equilibria, showing up some differences with respect to conventional aspect ratios [43]. Although this model is imprecise for extreme shapes on TCV ($\delta < -0.6$), a deformable linearized model continues to give excellent agreement [44].

Work is progressing on linking equilibrium control and kinetic control. Integration of the profile control system with the equilibrium control is highly desirable for the following reasons. When switching on and off heating and current drive actuators, the plasma profile parameters β_p and l_i experience large fast variations which act as disturbances; the overall control performance would be improved by integrating the two separate control systems to account for the interactions between them. The q-profile is strongly affected by the total plasma current and the shape of the boundary; independent requests of the two control systems can cause conflict between separate control systems. At JET, a multi-variable model-based technique is used to control the current and the pressure profiles in plasmas with internal transport barriers [45, 46] (see figure 7). With only the three heating and current drive actuators (LH, NBI and ICRF heating and current drive) satisfactory control of the q-profile can be achieved, with the possibility of simultaneously controlling the plasma current and the pressure profiles. Plasma pressure and current density profile response models are being based on system identification carried out on experimental data [45]. However, an effort should be made to derive *a priori* models of the plasma profile response to various inputs in order to have the possibility of applying simulation and controller design procedures to future tokamaks such as ITER. This requires a full understanding of transport and is not yet feasible.

4.1.2. Magnetic control in ITER.

The main features of ITER plasma current, position and shape control system are described in [47, 48] and in chapter 3.7.4.1.3 of [2]. The double wall (each 60 mm thick) stainless steel vacuum vessel, shown in figure 8, provides the main contribution to the passive stabilization of plasma vertical displacements. Another important element of the plasma passive stabilization is the set of toroidally continuous conducting structures supporting the lower outer blanket modules. These structures improve the up/down symmetry of the conducting structures as they couple well with any plasma vertical motion and in particular
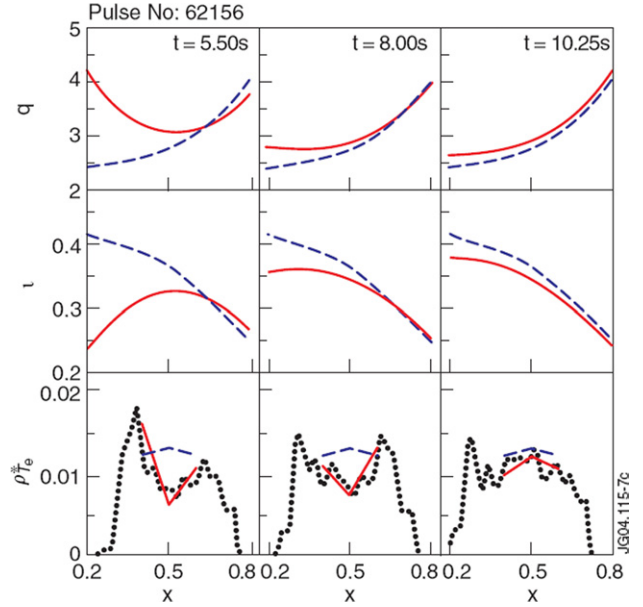

Figure 7. Measured (——) and target profiles (- - - -) for q, $\iota = 1/q$ and $\rho_{Te}^* = \rho_s/L_T$, for JET pulse 62156 ($B_T = 3$ T, $I_p = 1.7$ MA, $n_e = 3 \times 10^{19}$ m^{-3}). For ρ_{Te}^*, the original profile has also been plotted ($\bullet$). Each column corresponds to one time, respectively, $t = 5.5$ s (start of control), $t = 8$ s and $t = 10.25$ s (end of control). Note: $\rho_{Te}^* = \rho_s/L_T$ is the lumped parameter used to characterize an ITB essentially proportional to the temperature gradient.

render the passive structure more symmetric with respect to the plasma. They in fact decrease the initial values of the plasma vertical displacement after plasma disturbance by about a factor of 2. The total toroidal resistance of the vacuum vessel with the blanket supporting structure is about 7.7 $\mu\Omega$. The time constant of the vacuum vessel mode associated with the plasma vertical displacement is about 0.2–0.3 s. The vertical instability growth times for plasmas of a representative inductive 15 MA scenario (Scenario 2 in table 3 of chapter 1 of this issue [49]) calculated with the codes EDDYCAL and ACCORD-3 using 3D models of the vacuum vessel are given in table 2. The value of internal inductance of these plasmas varies within the design limits [0.7, 1.0].

The most unstable is the plasma at the start of current flat-top (SOF), when the value of β_p is low. At the start of burn (SOB), the instability growth time of the plasma with the reference value of l_i (0.85) is 0.119 s.

The quasi-symmetrical configuration of the ITER PF system allows the use of one ac/dc converter dedicated to plasma vertical stabilization (VS), which is connected to the coils PF2–PF5, as shown in the simplified schematic of figure 9. Compared with the main ac/dc converters connected in series with each coil, the VS converter has four times higher output voltage and shorter response time. The VS converter carries only the imbalance current, which is the algebraic sum of the currents in the coils PF2 through PF5.

In order to make optimal use of these features, a control scheme with two feedback loops acting on different time scales has been designed. In the fast VS loop, the feedback algorithm determines the voltage of the VS converter using as input the vertical velocity of the plasma current centre. The slow feedback loop provides control of plasma current and shape
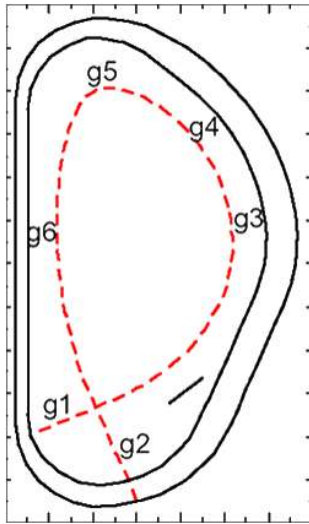
Figure 8. Plasma of ITER Scenario 2 (- - - -), double wall vacuum vessel (——), toroidal conducting element of the blanket support and 6 controlled gaps (g1, ..., g6).

Table 2. Growth time of plasma vertical instability, τ, for plasmas of Scenario 2.

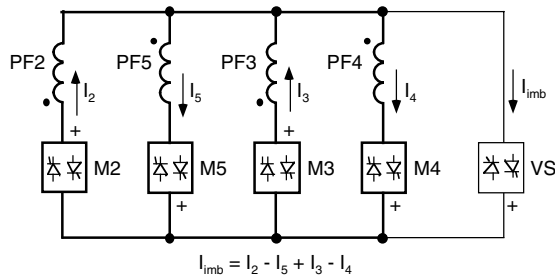| Scenario phase	l_i	β_p	τ (ms)
SOF	0.7	0.1	105
SOF	0.85	0.1	84
SOF	1.0	0.1	64
SOB	0.7	0.65	165
SOB	0.85	0.65	119
SOB	1.0	0.65	90

$$I_{imb} = I_2 - I_5 + I_3 - I_4$$

Figure 9. The vertical stabilization (VS) circuit.

by acting on the CS and PF coil main converters. Plasma shape control in divertor configurations is realized with the control of the six gaps between the separatrix and the plasma facing components. The locations of the gaps are shown in figure 8. The control system aims also at minimizing the steady state current deviations, in the VS converter and in the main CS and PF converters, from their reference scenario values. The resulting closed loop bandwidth of the fast loop is about $20\,\mathrm{rad\,s^{-1}}$, whereas the slow loop bandwidth is about $1\,\mathrm{rad\,s^{-1}}$; the two loops are therefore well decoupled in the frequency domain.

The control system maintains the specified plasma current, the position and the shape in spite of slow evolution of plasma parameters during the scenario, rapid changes in the additional heating and non-inductive current drive, fast transient disturbances to the current and pressure profiles

produced by MHD activity (plasma disturbances) or by the H- to L-mode transition. The underlying physics basis and characteristics of the plasma disturbances affecting the plasma current, the position and the shape varying l_i and β_p: minor disruptions (MD), ELMs and sawteeth, are presented in chapter 3 of the ITER Physics Basis [50]. Two types of large-scale recoverable plasma disturbances are used for the design of the controllers and for their studies in the inductive scenarios.

1. MD1: an instantaneous l_i drop of 0.2 ($l_{i0} - 0.5$) without recovery simultaneous with a β_p drop of $0.2\,\beta_{p0}$ followed by a 3 s exponential recovery.
2. MD2: an instantaneous β_p drop of $0.2\beta_{p0}$ followed by a 3 s exponential recovery.

Minor disruptions of the first type are more demanding for the plasma control. For plasmas with the nominal position and the shape having the value of l_i within the design limits, the MD1 cause plasma downward vertical displacements with the initial value of about 10–20 mm. For example, in Scenario 2, the SOF plasma with $l_i = 1$ jumps downwards by 14 mm (derived using the PET code with a 2D model of the vacuum vessel).

Linear plasma models were used for design of the controllers and for preliminary analysis of the controller performance in the case of MDs. Simulations were provided for the key states of the Design Scenarios 1, 2 and 5 (see chapter 3.7.4.1.1 of [2]) with the various plasma equilibria having different l_i. The main results of the linear model simulations, obtained for the 2D model of the vacuum vessel, can be summarized as follows. The settling time of the gap control, defined as the time needed for the deviation of all the gaps to become less than 10 mm, is about 5–20 s. The maximum displacements of the separatrix legs towards the divertor dome is 100 mm for the inner leg (gap 1) and 70 mm for the outer leg (gap 2). For the controllers having a plasma shape control settling time of 5–10 s, the maximum displacement of the separatrix towards the first wall is about 30 mm for the gaps 3 and 4, whereas for the gaps 5 and 6 it is about 90 mm. All these displacements are within the acceptable limits.

In addition to the linear plasma models, free plasma boundary time varying codes MAXFEA, PET and DINA [51, 52] have been used in order to analyse the non-linear performance of the controllers. The study performed with these codes demonstrated the required performance of the ITER PF system.

As an example, figure 10 shows variation of the control parameters and the coils currents, voltages and powers in the PET simulation of the plasma current, the position and the shape control during MD1 at the SOF of Scenario 2 for the plasma with $l_i = 1.0$. Conservation of the magnetic helicity was assumed in the calculation of an initial step of the plasma current after the fast drop in plasma internal inductance (in this case by 0.1). The control system recovers the plasma current, the position and the shape after minor disruption in about 5 s. All currents, voltages and powers are within the design limits.

When the value of l_i increases, the outer separatrix may dangerously approach the inner one. Reduction of the distance between the separatrices to about 1 cm (in the equatorial plane, outboard) may result in unacceptably high heat loads on the first wall near the upper X-point. Active cooling of this region
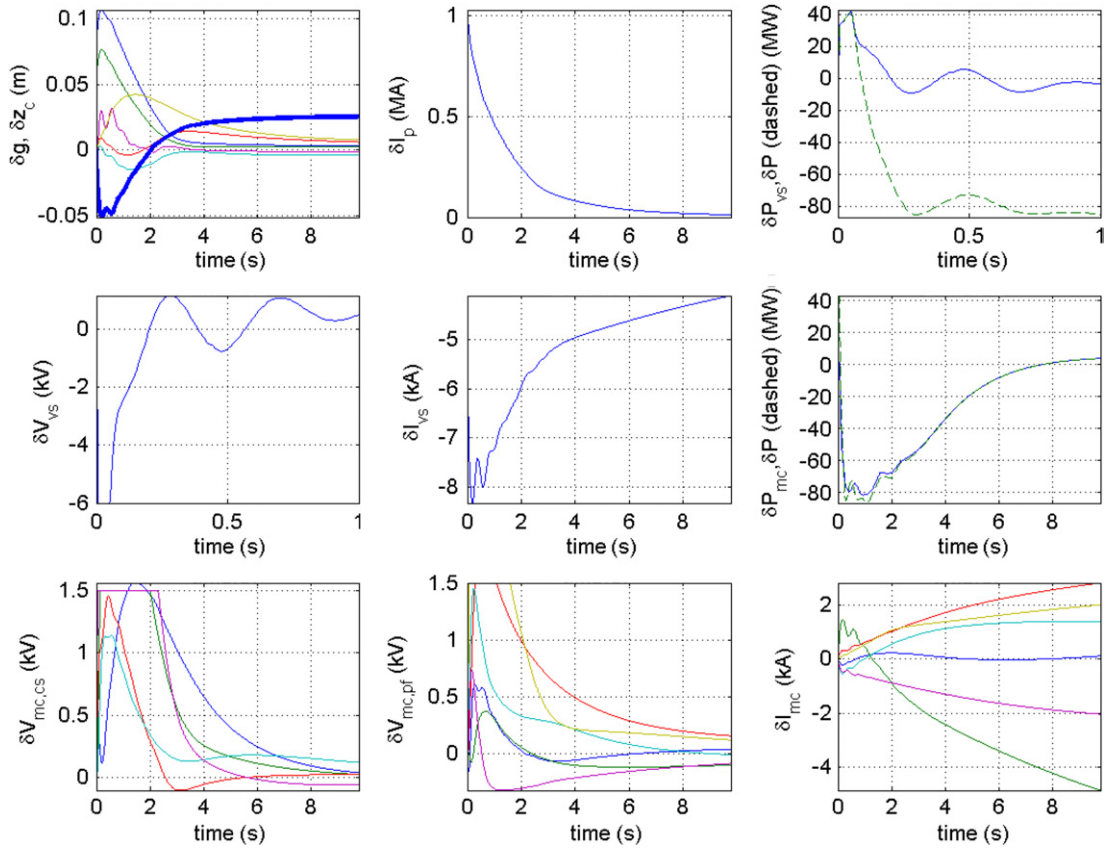
Figure 10. PET simulation of plasma current position and shape control during minor disruption (MD1) at the SOF in Scenario 2 for the plasma with $l_i = 1$. The figure shows the displacement of plasma current centre, δz_c, (bold blue line); the displacements of controlled gaps, δg, (g1—blue, g2—green, g3—red, g4—cyan, g5—magenta, g6—yellow lines); the variation of plasma current δI_p; the voltage of VS converter, δV_{vs}; the voltages of main converters of the CS coils, $\delta V_{mc,cs}$, (CSU2—blue, CSU1—green, CS1—red, CSL1—cyan, CSL2—magenta lines); the voltages of main converters of the PF coils, $\delta V_{mc,pf}$, (PF1—blue, PF2—green, PF3—red, PF4—cyan, PF5—magenta, PF6—yellow lines); the variation of current in the VS converter, δI_{vs}; the variations of currents in the main converters of the PF coils, δI_{mc}, (PF1—blue, PF2—green, PF3—red, PF4—cyan, PF5—magenta, PF6—yellow); the total active power, δP, (green dashed line); the power of VS converter, δP_{vs}, (solid blue line); the total power of main converters, δP_{mc}, (solid blue line).

is very problematic and therefore additional protection of this region is not planned. Taking into account the accuracy of the magnetic reconstruction of the separatrices (about 1–2 cm) and static errors of the gaps control (about 1 cm), the design criterion of the quasistatic control of the separatrices separation is 40 mm. To fulfil this criterion, a controller was designed which, in addition to the control of plasma current, position and shape (six plasma-wall gaps), does not allow the gap between separatrices in the equatorial plane to be less than 40 mm [2].

Several studies have been carried out to estimate the effect of the vacuum vessel ports and other conducting structures on the plasma current, position and shape control [2]. Details of the model of the conducting structures become more important when the stability margin reduces. The results can be summarized as follows. The vacuum vessel ports decrease the growth time of plasma vertical instability by 15–20% (depending on the stability margin). Table 3 shows the instability growth times calculated with CREATE-L models having 2D and 3D models of the vacuum vessel.

For reduction of the forces acting on the blanket modules during disruption to the sufficient level, the blanket modules have cuts decreasing the currents induced in them. As a result, the blanket modules have a time constant more than 10 times lower than that of the vacuum vessel. Because of

Table 3. Growth time of plasma vertical instability (in ms) calculated for plasmas of Scenario 2 with 2D and 3D models of the vacuum vessel (CREATE-L).

Scenario 2 plasma	2D model	3D model
SOF: $l_i = 0.7$, $\beta_p = 0.1$	137	117
SOF: $l_i = 0.85$, $\beta_p = 0.1$	109	92.6
SOF: $l_i = 1.0$, $\beta_p = 0.1$	88	74
SOB: $l_i = 0.7$, $\beta_p = 0.65$	195	169
SOB: $l_i = 0.85$, $\beta_p = 0.65$	152	131
SOB: $l_i = 1.0$, $\beta_p = 0.65$	120	104

this, the blanket modules provide a minor stabilizing effect. For example, at SOF in Scenario 2 for the plasma with $l_i = 1$ they increase the instability growth time by about 2.6% (CREATE-L model). The study provided has also shown that the intercoils structure of the toroidal field coils, the cryostat and the outer-cryostat structures also insignificantly affect the plasma current, position and shape control [2].

Possible abnormal operational regimes, due to failure of one PF converter or current saturation in one PF coil, were studied at a preliminary level and reported in [2]. The analysis concludes that in all key states of Scenario 2 it is possible to counteract a minor disruption and to restore the plasma

shape in 20 s, even if one of the PF converters fails (produces zero voltage). The shape control accuracy is affected by the failure, but the controller limits the plasma–wall interaction to reasonable values. A strategy to counteract the possibility of current saturation in the PF coils was also developed. An anti-saturation controller, changing the reference signals for the gaps, was proposed. The simulations performed with such a device, both on linear and non-linear models, show the effectiveness of such a system in keeping the coil currents far from their saturation limits with a moderate deterioration on the shape control accuracy. A new approach to handling saturation of the power supply voltages has been developed and tested using the standard ITER linearized models and the previously developed controllers [53, 54].

Developing feedback control algorithms which are more or less expensive in terms of ac losses was taken up as an ITER design task and a simplified fast estimate of the ac losses during an ITER pulse was developed [55]. The general result was as expected, namely, that reducing the speed of the controllers not only reduces the ac coupling losses but also the performance when rejecting sawtooth or ELM perturbations. For short duration ITER discharges, the gain is small, but can become useful if long discharges have large regular perturbations.

4.2. Plasma performance control

4.2.1. Performance control in present tokamaks. Active control of the plasma performance control in experiments today is focused mainly on control of MHD modes (sawteeth, neoclassical tearing modes or resistive wall modes), control of the current density profile, control of the pressure profile in scenarios with internal transport barriers and control of the edge of H-mode plasmas so as to demonstrate performance with tolerable ELMs. These topics are covered in other papers. What remains to be covered in this section is (i) the control of global parameters to optimize performance close to MHD limits, density limits or instability limits, (ii) the identification of the confinement regimes as input for the control algorithms or the control strategies and (iii) the control of temperature, density and impurity profiles.

Control of global parameters to optimise performance. Most experiments use control of global plasma parameters to optimize performance. The main parameters are density, stored energy (β or D–D reaction rate) and radiative power. The main actuators for the density are fuelling, plasma shaping and (divertor) pumping, and for the stored energy (or related parameters) mainly the neutral beam heating. The radiative power is controlled through a combination of impurity dosing and input power variation. While control of the plasmas density is seen as basic plasmas control, the performance can be related to line averaged density compared with the Greenwald density and the neutral pressure in the main chamber and the divertor chamber. Control of the stored energy requires more complexity as this is in some cases linked to the (empirical) knowledge of safe operation close to MHD limit boundaries. This is emphasized by results from DIII-D [56], JET [57] and ASDEX Upgrade [58], demonstrating operation at maximum beta under stationary conditions in hybrid scenarios. Control of the radiative power has to cope with different time constants from impurity diffusion or recycling and possible confinement

transitions, as recognized in the optimization of discharges with high radiation fractions in JET [59, and references therein].

Performance regime identification. The ability to determine different confinement regimes in real time is of increasing importance for performance control. For example, a simple control system for the edge density may continue to increase the fuelling rate when the H-mode near the Greenwald density limit is lost, augmenting the confinement loss rather than reducing the fuelling so as to restore the good confinement properties. Hence, the ability to recognize the transition from the L-mode to the H-mode or from the H-mode to the improved H-mode reliably from a conveniently small number of measurements in real time is of increasing importance for machine control.

Discriminant analysis has been applied to the regime identification of plasma discharges in the ASDEX Upgrade tokamak [60]. Discriminant analysis is concerned with the problem of determining a rule from a data set of observations that have been classified into distinct groups, which allows the group membership of a subsequent observation to be decided. A sufficiently large training data set for prediction can be obtained from a limited amount of development discharges. An observation consists of a set of plasma parameters averaged over a time slice in a discharge. Several observations may be obtained from a single discharge. An analysis seeking the two, three, four or five plasma variables from all variables in the data set whose linear combination yielded the minimum prediction failure rate of a L-mode or a H-mode was carried out. Using five plasma variables, L-mode and H-mode phases have been successfully identified in real time at ASDEX Upgrade. An illustration is given in figure 11, showing the time evolution of the whole discharge. Detailed analysis shows that the prediction for the H-mode from discriminant analysis at $t \sim 1.6$ s is about 20 ms after the actual H-mode transition indicated by the D-alpha emission measurements. This is an acceptable error for control purposes as the energy confinement time is typically 100 ms in ASDEX Upgrade. With five variables a failure rate of 1.3% for predicting the L-mode and the H-mode confinement regimes was achieved. What is relevant here is that the method works with high reliability and is fast enough to allow control schemes to adapt to the change in regime. The algorithm used in figure 11 keeps the last state when the input data become invalid (L-mode, when the discharge is finished). A more modern version of the regime identification sets the regime to 'not known' when the input data become invalid. Applying discriminant analysis to other regimes, such as the improved H-mode at ASDEX Upgrade (a candidate for hybrid operation in ITER, see chapter 6, section 3, of this issue [4]), a failure rate of 5.3% is achieved with five plasma parameters (the failure rate for distinguishing between the H-mode and the improved H-mode confinement regimes).

Control of profiles. Recently plasmas control systems have developed enough to obtain active control of the plasma profile using a variety of real time diagnostics [61]. Although demonstration of control is mainly in discharges with internal transport barriers [45], other results deserve attention. In DIII-D feedback control of the electron temperature at a single
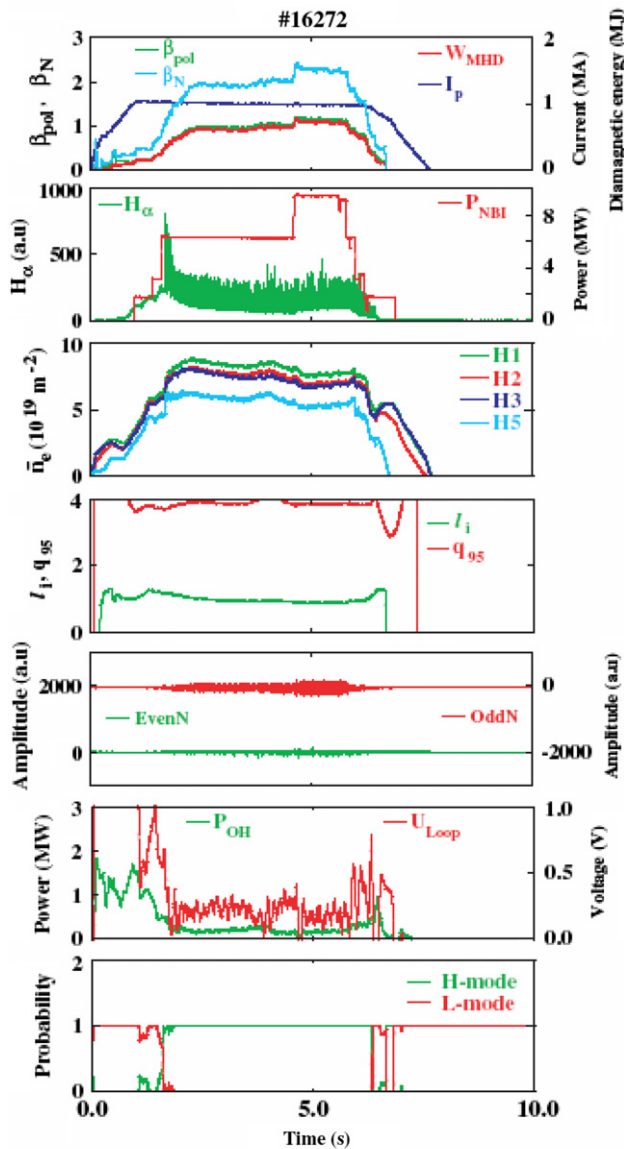
Figure 11. Overview of plasma parameters in an ASDEX Upgrade discharge with the regime identification probabilities calculated for the L-mode (red) and H-mode (green) in the bottom-most plot. The frequentist approach is used to calculate the probabilities (from [60]).

off-axis point enabled selection of current density profiles at the start of the flat-top for a range of plasma densities [62], aiding in the reproducibility of high performance discharges. Plasmas with peaked density profiles have typically higher confinement; however, control of excessive density peaking is required to avoid neoclassical tearing modes, accumulation of high-Z impurities in the plasma centre. Also broader density (pressure) profiles give increased stability against low n-instabilities at high beta. Various experiments demonstrate that control of the density profile can be achieved through careful selection of the heating deposition profile [63,64]. Here the explanation is that the reduction of the heating to the core reduces the turbulent driven transport in standard H-modes. Provided the thermal and the particle transport are linked

together, this reduces the outward particle flux compared with the inward particle fluxes resulting in more peaked density profiles (see transport in chapter 2 of this issue [65]). Similarly the control of impurity accumulation has been demonstrated by applying central heating to the plasma. This also includes regimes with improved core confinement as the hybrid scenarios at ASDEX Upgrade where the accumulation of tungsten from the plasma facing components was controlled using central ECRH as well as the quiescent double barrier mode (QDB) in DIII-D where the density peaking and the central impurity density were reduced using ECRH deposited near the axis. In ITER, central alpha heating could avoid excessive density peaking or impurity accumulation along the lines described above, although control of the density profile and central impurity density may be required in order to reach the condition with dominant alpha power heating.

4.2.2. Performance and burn control in ITER. This section describes performance control in ITER inductive scenarios, although many of the issues are also relevant to steady state operation. At the simplest level, the key kinetic attributes of the core plasma control are density, temperature, impurity content, current density and fusion power. The key attributes of the divertor plasma control are density, temperature, impurity content, radiation power in the core and the divertor region and the power to the divertor target. Also important is the control of ELM amplitude, which is discussed in chapter 4 of this issue [66]. Among these attributes, the most important attributes to be controlled are fusion power, P_{FUS}, and the power to the divertor target plates, $P_{Divertor}$. In addition also the power across the edge pedestal region, P_{LOSS}, should be controlled for the transition from L- to H-mode (in the start up phase) and H- to L-mode (in the shutdown phase).

To control the above three variables (P_{FUS}, $P_{Divertor}$ and P_{LOSS}), there are four main actuators: (1) additional heating power P_{ADD}, (2) DT gas or pellet injection rate, (3) high-Z impurity (for example, argon) injection rate and (4) pumping rate.

The control system is non-diagonal as every input variable has an effect on every desired output. However, the strongest effect on fusion power is given by changing the particle density. Additional heating has a major impact on both fusion power and L- to H-mode transition control, whereas heavy impurity injection has its main impact on the local radiated fraction in the divertor region.

Control of fusion power in high-Q operation by impurity seeding can be considered as an example of performance control in ITER. The control of fusion power excursion is one of the most important issues in the fusion reactor. Studies have shown that burn control can be made in plasmas with Q values in the range $\sim$10 [67] In the case of high-Q or ignited operation, fusion power cannot be controlled only by the additional heating power. In this case, high-Z impurity seeding or density control has been considered as one of the means for burn control. Figure 12 shows a simulation where the suppression of the fusion power excursion is achieved by impurity injection. Here, $I_p = 17$ MA, $\langle n_e \rangle = 1.18 \times 10^{20}$ m^{-3} ($\langle n_e \rangle / n_G = 0.87$), $\tau_{He}^*/\tau_E = 3$, $H_{H98(y,2)} = 1.0$ and, a means of creating an ignition condition, a heating power P_{ADD} is added from 10 to 13.7 s. The dotted line denotes the case
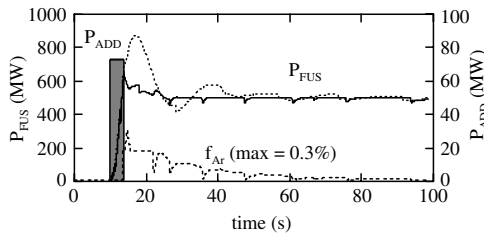
Figure 12. Suppression of fusion power excursion by impurity seeding in ignited operation. Here, $I_P = 17\,\text{MA}$, $\tau_{He}^*/\tau_E = 3$, $H_{H98(y,2)} = 1.0$ and 73 MW of additional heating power (P_{ADD}) is added from 10 to 13.7 s. Solid line: with argon (Ar) impurity seeding, dotted line: without impurity seeding.

without impurity seeding. In this case, although the increase in fusion power is limited by helium ash accumulation, a large overshoot of fusion power is observed. In the case of the solid line, argon impurity (Ar) is injected and the overshoot of fusion power is suppressed. The density control can be instrumental for performance control [68], but the characteristic time tends to be longer than impurity injection

4.2.3. Specific control issues for steady state operation.

(For a more extensive overview and figures see chapter 6, section 5, in this issue [4].) Steady state conditions with high fusion gain Q require (i) control of confinement, for most advanced scenarios this is closely related to the control of the safety factor and pressure profiles, (ii) control of the (global) plasma stability at high beta (typically $\beta_N > 2.5$), (iii) the control of α-particles losses via collective instabilities and (iv) control of particle exhaust to ensure acceptable levels of helium or other impurities. In addition, most control parameters for conventional pulsed operation will also be used in steady state operation. These include the total plasma current, the plasma cross-section and shape, vertical position and the loss power to the divertor.

This level of active control of a plasma discharge requires the use of a wide range of real time sensor parameters and appropriate actuators [69, 70]. The simultaneous control of these quantities with different characteristic time scales and response times of the actuators available complicates the requirements for real time control of steady state discharges. Hence, essential for the preparation of the scenarios and for the design of the controllers are the simulations of real time control experiments using suitable transport codes presented in chapter 6, section 6 of this issue [4].

Several tokamaks have now developed comprehensive real time measurement networks capable of issuing most of the data required for the control of steady state discharges, in particular JET [45], Tore Supra [71], JT-60U [72] and DIII-D [73]. Other plasma parameters relevant to steady state control are also calculated online by dedicated codes. For the computation of the current and q profiles, DIII-D and JET have for example developed real time equilibrium codes EFIT [19] and EQUINOX [74], capable of integrating internal flux measurement from infra-red polarimetry or MSE measurements. The inferred magnetic flux can also be used to map the kinetic profiles to get the pressure profile. JET has also developed an internal barrier criterion using the

data from the ECE diagnostics to calculate the quantity ρ_{Te}^* that should be in excess of 0.014 to detect an ITB [75]. The parameter $\rho_{Te}^* = \rho_i/L_{Te}$ (where L_{Te} is the electron temperature gradient length) is inferred from the diamagnetic part of the power balance equation and characterizes the ITB strength using the temperature data. In various experiments the central controller units are also being upgraded to facilitate the routine use of so-called multi-input multi-output (MIMO) control schemes, which are required for simultaneous current and pressure profile feedback control [76]. The recent improvements in diagnostic reliability and the rapidly growing capabilities of computers and communication networks have recently enhanced the prospect for multi-variable control and the combination of different plasma parameters in control schemes.

From single variable control to multi-variable control in steady state scenarios. Initially real time control systems were used to control one plasma parameter with one actuator only. This enabled one to maintain the performance (and avoid major instabilities) of advanced scenarios in various experiments by using feedback control of the stored energy or neutron rate through the modulation of the neutral beam power [45, 73, 77–79].

Long-pulse operation has been demonstrated in Tore Supra [71] by using two proportional feedback loops. The first loop controlled the flux on the plasma boundary through the variation of the voltage on the Ohmic power supply while the second loop controlled the total current by lower hybrid power modulation [80]. However, the relationship between a given actuator and a parameter selected for control is seldom straightforward; parameters and actuators are most of the time coupled with each other. Experiments have started using the simultaneous feedback control of multi-variables. In JT-60U for example, control of ELMy H-modes using three major control parameters was demonstrated: the operating density, the neutron rate and the divertor radiation power [77]. These parameters are controlled by the gas puffing near the top of the vessel, gas puffing in the divertor region and the NBI power. Another example from JET, following single variable feedback control of radiation in TEXTOR [81] and JT-60U [82], shows the simultaneous control of the confinement and radiation level for the duration of 6 s [83]. Argon and deuterium puffing have been used as actuators in a dual feedback control of both the enhancement factor $H_{98}(y, 2)$ and the radiation level in high triangularity discharges. The actuators of the feedback control are the deuterium puff rate and the argon-seeding rate. This leads to the highest possible density for a given confinement quality. The feedback scheme uses a 2×2 control matrix, which is calculated from open-loop shots with pre-programmed D and argon puffing and remains valid around a chosen operational condition. A similar scheme has also been used in DIII-D, where both bolometer measurements and the spectrometer signal for an impurity line have been used to provide diagnostic inputs and the puff rate of an impurity gas and divertor cryogenic-pumping of the particle exhaust were used as actuators [84].

Feedback experiments of advanced tokamak scenarios using profile control. The control of advanced tokamak regimes

is regarded as a challenge in particular because of the non-linear coupling between the current density and the pressure profile illustrated by the interplay between bootstrap current and pressure profiles. Recent experiments have focused on maintaining pressure and current profiles at their optimum (stable) shape in the operation of a steady regime. Preliminary experiments in several devices concentrated on separate feedback control of the current and pressure profiles. In DIII-D feedback control of the electron temperature at a single off-axis point, enabled selection of current density profiles at the start of the flat-top for a range of plasma densities [85], aiding in the reproducibility of high performance discharges. Other examples of the control of the central q value in DIII-D are given in [86] using electron cyclotron heating and neutral beam injection. For simultaneous control of the q-profile and pressure profile, the method used at JET is to build a linear Laplace response model around the target state to be controlled [87, 46]. The static transfer matrix can be determined experimentally using step or modulation experiments of the actuators. This model-based technique has been applied to control the q-profile during the high power heating phase of plasma pulses, using three actuators (i.e. LHCD, NBI and ICRH) [46]. During recent campaigns in JET, experiments have been conducted achieving for the first time the simultaneous control of the current density and electron temperature profiles in ITB plasmas. The distributed-parameter version of the algorithm was implemented using 3 actuators (LHCD, NBI and ICRH) and 8 output parameters. The profiles are projected upon 5 cubic-spline basis functions for the inverse safety factor, $\iota(r)$, and 3 piecewise-linear functions for the normalized electron temperature gradient profile, $\rho_{Te}^*(r)$. Real time control of different target q-profiles—from monotonic to reversed shear ones—while simultaneously controlling the profile of the electron temperature gradient was demonstrated (see figure 7) [88, 46]. The response of the controller has also been simulated over longer time scales using the JETTO transport code. Comparisons with the actual experiments are qualitatively satisfactory [89].

A new feature of ITER is the small number of NBI sources. The power of each source can be adjusted by about ±10% for the flat-top control. Termination of one beam will create a drop of about 50% in heating power and might change the regime, e.g. loss of H-mode. This feature must be studied in simulations and should be studied in present experiments.

4.3. Plasma control simulations in present tokamaks and ITER

This section discusses full simulations of tokamak discharges. A variety of techniques have been used for many years, with different purposes. Conventionally, plasma equilibrium control simulations use linearized models with little or no respect for plasma resistance or current diffusion and no transport physics. The linearized plasma response model of JET has been used for closed loop simulations, providing a reliable starting point for the design of the new XSC, as mentioned; TCV and DIII-D have demonstrated the quality of their linear models for flat-top closed loop simulations. Transport modelling, both interpretative and predictive, tends

to use fixed or prescribed evolution of the plasma equilibrium. There has always been an interest in attempting to model a full tokamak discharge, from the control actuator inputs through to the plasma profile evolution. Up to now, such work has concentrated on the TSC and DINA codes, which solve the evolution due to plasma transport and flux diffusion in the coordinates of the flux surfaces and the evolution of the flux surfaces in a rectangular grid. Such simulations are expensive in computer time, but have become more and more tractable as computers have speeded up. This section therefore concentrates on the full discharge simulation work and looks forward to the simulations which could be performed as part of the ITER exploitation.

4.3.1. Simulations of present tokamaks. For simulations in which the non-linearities are important, when the equilibrium is evolving significantly, work has progressed using full non-linear simulations, of which the DINA 1.5D code [51] and the TSC code [90] are the two most widely used plasma simulators. Their avowed aim is to develop reliable predictive capability for use on future devices to study plasma equilibrium control and plasma kinetic control, especially in conditions in which the latter influences the former. These codes were validated and used in many tokamaks. For example, validation of the DINA-CH version of the DINA code has proceeded along several lines. First the closed loop responses to voltage perturbations were successfully tested on TCV [91]. Next a series of vertical displacement events were chosen for modelling the plasma displacement in the particularly inhomogeneous vacuum field structure of TCV, showing initial exponential growth with subsequent slowing (the so-called *S* curve) evolution of $z(t)$, reflecting the reduction of the vertical field decay index ($-R/B_z \times \mathrm{d}B_z/\mathrm{d}R$) as the plasma moved further away from the equilibrium point [92]. Fully ECCD non-inductive discharges were simulated, as well as high bootstrap current fraction discharges [93]. One important detail here is the real-space dependence of the ECH/ECCD deposition, not explicitly imposed on a flux surface, but in a small volume in real space. The evolution of the equilibrium then itself determines on which flux-surface the current is driven and the heat is deposited. A fixed boundary simulation cannot do this and an imposed varying boundary cannot be used in the predictive mode. The ECCD simulations, using simple empirical transport models, were found to be unexpectedly sensitive to plasma transport during the fast evolution of the equilibrium, exposing the dynamical evolution of the plasma shape as a possible discriminator for transport modelling, for the first time motivating a more complete study of transport modelling in DINA-CH. To make simulations of existing discharges agree closely, it was essential that the simulation should precisely reproduce the Ohmic flux swing. Instead of trial and error, a feedback loop was closed around the simulation, forcing the loop voltage to follow the discharge, by adapting the resistance anomaly attributable to Z_{eff}.

On DIII-D work was also carried out on full simulations using DINA to validate the code against experimental data [94], especially disruptions not yet covered by DINA-CH. On ASDEX Upgrade, TSC was used to simulate the effect of the neutral point (where a step in β_p does not lead to a jump in Z) on disruptions [95]. Furthermore, a specific ramp-up of the

JT-60U reversed-shear discharge was nicely reproduced by TSC with models of ITB and associated bootstrap current. A fast and strong ITB built-up near the plasma centre was demonstrated to cause an over-driven bootstrap current inside the ITB region, eventually leading to a formation of current hole near the magnetic axis as experimentally observed in JT-60U [96].

4.3.2. Evolution of complete discharge simulators for ITER. Work has been carried out in parallel on TCV and on DIII-D to develop further and validate full discharge simulators, using both linear models and the DINA code. Both groups chose independently to interface DINA via the open-architecture offered by Matlab-SIMULINK and used this software for the linear simulations, incorporating realistic models of the diagnostics, controllers and power supplies. TCV developed a collaborative version of DINA-CH which simulates TCV, ITER and MAST tokamaks using the same DINA code version [12]. Plans include incorporation of the exhaustively tested TCV equilibrium to the diagnostic mapping code, to allow complete simulation of all diagnostic equipment and thereby realistically close the kinetic control feedback loops. The DIII-D approach has been similar, and in both approaches, the approach has allowed the use of either a linear plasma response model or the non-linear DINA model.

4.3.3. Further developments required for plasma control in ITER. The typical methods to be used for controlling ITER plasmas have been well developed on many devices. Integration of the different techniques into a full and flexible system will require effort, allowing many of these different approaches to be implemented according to the experimental programme.

Some features of control have been developed in isolation, some already mentioned, and will need incorporation into the overall architecture, such as bump-less transitions between controller phases with different architecture controllers, minimization of ac losses, handling of voltage saturation, handling of current saturation, handling of power supply failures, handling soft stops and minimizing the instantaneous power requirements. Most of these issues have some experimental support and all have received attention by modelling.

Refinement of a flight simulator capable of integrating all the features of ITER plasma control is an essential challenge for several reasons. Evaluating the ITER control systems before a discharge will require detailed simulation capability to verify a proposed operational plan to demonstrate that it satisfies the ITER design specifications prior to discharge start-up, especially during initial operation but also during routine operation. This 'flight simulator' should therefore have the capacity to validate the effects of any proposed modifications to the control systems on the overall device, to avoid losing operational time due to non-optimal adjustments common on present-day tokamaks. However, since ITER will explore new plasma regimes, not necessarily accurately modelled in the flight simulator, allowance must be made for simulating unexpected conditions.

This operational requirement of a 'flight simulator' is distinct from the 'numerical tokamak' goal whose purpose is to model the complete behaviour of the plasma discharge itself from *ab initio* assumptions and to validate or improve our physics understanding. The latter will ultimately represent our accumulated understanding of tokamak physics, on which extrapolation to other devices can be made. The former represents our understanding of the functioning of a complex engineering project. Its purpose is to simulate what is important for the development of new experimental scenarios and to avoid lost time due to not mastering the complexity of ITER.

To demonstrate the applicability of a particular architecture, a prototype ITER plasma control system (PCS) was constructed based on the DIII-D PCS, along with a simulator of the ITER tokamak poloidal shape control system. The ITER simulator consisted of a linearized ITER plasma and conductors model in the state space form and models of the proposed ITER power supplies as specified by ITER design documents. An integrated shape, stability and plasma current control algorithm was developed using the ITER plant model, then implemented in the ITER PCS. Preliminary ITER hardware in the loop simulations have been conducted. Models of non-axisymmetric conductors, actuators and heating have also been implemented in multiple Simulink models, but not yet incorporated into a single integrated model [97, 98].

It is expected that the evolution of a reliable 'flight simulator' will be significant over the next few years, allowing more tokamaks to be simulated in more elaborate scenarios, validating a small number of codes in preparation for ITER exploitation. Work is already underway to integrate different codes, such as MHD stability estimates and edge transport simulations, into a unified structure, without creating a gigantic single code which would become unmanageable.

5. Summary

Plasma operation and control for ITER are based on the proven techniques used in present-tokamak experiments. ITER will operate as a pulsed experiment, albeit with very long pulses. Safety issues are relegated to specific systems which detect off-normal events and react accordingly. Magnetic control will be conventional, but with demanding tolerances. Kinetic control will be very important and combining the kinetic and magnetic control into a single control system is already underway in existing experiments. Although most of the control issues in present tokamaks are aimed at improving the performance of pre-programmed discharges, a great deal of effort will have to be dedicated to the optimization aspect of control in ITER. This will be one of the physics-based challenges. The methodology for doing this can already be established in existing tokamaks, except for the final element of the role of the alpha power and scaling of the transport coefficients, for which we depend on simulations and on experience gained operating ITER itself.

The large size of ITER brings an immediate challenge, namely achieving effective and reliable breakdown. Although calculations based on the existing experience from all our tokamaks suggest that with the assumed impurity mix, breakdown with just the induced electic field should be achievable, the margin appears to be rather too low for comfort and breakdown assisted by 2 MW of ECH is foreseen. This

should help not only achieve breakdown reliably, but also possibly to affect its location.

The physics basis for magnetic control of the plasma position and shape has not evolved significantly in the last few years, but has been the subject of continued improvement and modelling. What has advanced impressively is the control of the internal radial profile of the plasma current, and the corresponding safety factor profile. This has required the triple development of estimated measurements of the q-profile, of actuators capable of modifying the q-profile in steady state, and of a sufficiently realistic model of the input-output actuator-profile relationship to produce reliable feedback controllers. These three requirements are starting to become available, although the most common weakness is presently an accurate estimate of the q-profile from the existing measurements. Work on the ITER project design itself has concentrated on the effects of departures from axi-symmetry and on improving the vertical passive stabilisation. Validation of the ITER magnetic control concepts is presently using a well tried mixture of linear and non-linear simulations and continues to yield positive judgement on the controllability of the magnetic systems.

Work on controlling the plasma performance has advanced significantly, especially in view of the requirement that ITER should operate close to the theoretical and empirical performance limits. In these conditions, the plasma control becomes more sensitive to the plasma regime. This is a significant difference with respect to magnetic control, in which the underlying model is robust. Maintaining stationary conditions close to operational limits is a challenge which is being met by many tokamaks, developing approaches which will be applicable, in style, to ITER. Controlling the internal transport barrier position and strength has attracted much interest recently, illustrating the combination between magnetic and kinetic control to achieve optimised plasma performance. After several years of development, originally transient phenomena are now being brought under control to achieve steady state conditions over timescales longer than the open-loop evolutionary timescales.

Burn control has progressed only on the simulation front, studying the effect of the available actuators. This example underlines the requirement of a suite of simulation tools for predicting the effect of different controller algorithms on the overall tokamak performance. A single tool would not be adequate and a mixture of linear and non-linear tools is required. Transport can be studied in many cases using fixed or prescribed last closed surface evolution, whereas a full simulation of the magnetic and kinetic feedback control circuits is only feasible in two codes, TSC and DINA, which are both developing in this direction. Reliance on simulators requires conviction in their validity and experiments to validate all these models are contributing to their reliability. During the next few years, these simulation tools will have to become integrated to form a 'flight simulator' as part of the pulse validation methodology for ITER.

Although physics basis of plasma operation and control is similar in ITER and present tokamaks, there is a principal qualitative difference. To minimise its cost, ITER has been designed with small margins in many plasma and engineering parameters, creating a significantly narrower operational space compared with present tokamaks. Furthermore, ITER operation is expensive and any component damage resulting from operational errors leads to a high repairing cost. These factors make it essential to use a maximum number of simulators and databases in the ITER global control system to increase reliability.

Acknowledgments

References

[1] ITER Physics Basis, Chapter 8: Plasma operation and control 1999 *Nucl. Fusion* **39** 2577

[2] ITER Technical Basis 2002 Plant description document Section 1.4.6: ITER plant operation and control *ITER EDA Documentation Series No 24* (Vienna: IAEA)

[3] Hender T.C. *et al* 2007 Progress in the ITER Physics Basis *Nucl. Fusion* **47** S128–S202

[4] Gormezano C. *et al* 2007 Progress in the ITER Physics Basis *Nucl. Fusion* **47** S285–S336

[5] Albanese R. and Villone F. 1998 *Nucl. Fusion* **38** 723

[6] Lloyd B. *et al* 1991 *Nucl Fusion* **31** 2031

[7] Lazarus E.A., Hyatt A.W., Jackson G.L. and Humphreys D.A. 1998 *Nucl. Fusion* **38** 1083

[8] Kajiwara K. *et al* 2005 *Nucl. Fusion* **45** 694

[9] Erckman V. and Gasparino U. 1994 *Plasma Phys. Control. Fusion* **36** 1869

[10] Tanga A. *et al* 1986 *Tokamak Start-up* ed H. Knoepfel (New York: Plenum) p 159

[11] Yoshino R., Seki M. 1997 *Plasma Phys. Control. Fusion* **39** 205

[12] Khayrutdinov R.R. *et al* 2003 *Proc. 30th EPS Conf. on Controlled. Fusion and Plasma Physics (St Petersburg, Russia)* vol 27A (ECA) P3.163

[13] Belyakov V.A., Lobanov K.M., Makarova L.P., Mineev A.B. and Vasiliev V.I. 2003 *Plasma Devices Oper.* **11** 193

[14] Senda I. *et al* 1996 Optimizing voltage wave forms of poloidal field coils at the plasma breakdown *JAERI-Tech* 96-016 Japan Atomic Energy Research Inst., Ibaraki, Japan

[15] Control Systems Design and Assessment 2004 Plasma initiation, ITER N 19 RI 13 R0.1 chapter 4.2.3

[16] Leonor V.M. and Zhogolev V.E. 2005 *Plasma Phys. Control. Fusion* **47** 903

[17] ITER Physics Basis, Chapter 2: Plasma confinement and transport 1999 *Nucl. Fusion* **39** 2175

[18] Hofmann F. *et al* 2002 *Nucl. Fusion* **42** 743

[19] Ferron J.R. *et al* 1998 *Nucl. Fusion* **38** 1055

[20] La Haye R.J. *et al* 2002 *Phys. Plasmas* **9** 2051

[21] Penaflor B.G., Ferron J.R., Johnson R.D. and Piglowski D. A. 2004 *Fusion Eng. Des.* **71** 47

[22] O'Brien D., Ellis J.J., and Lingertat J. 1993 *Nucl. Fusion* **33** 467

[23] Sartori F., Cenedese A. and Milani F. 2003 *Fusion Eng. Des.* C **66–68** 735

[24] Kurihara K. 1993 *Nucl. Fusion* **33** 399

[25] Kurihara K. 2000 *Fusion Eng. Des.* **51–52** 1049

[26] Kurihara K. 1992 *Fusion Eng. Des.* **19** 235

[27] Kurihara K. 1998 *Fusion Technol.* **34** 548

[28] Lennholm M. *et al* 1997 *Proc. 17th Symp. on Fusion Engineering (San Diego, USA)* p 539

[29] Hofmann F. *et al* 2002 *Nucl. Fusion* **42** 59

[30] Sartori F. *et al* 2003 *Fusion Eng. Des.* **66–68** 727

[31] Sihler C. *et al* 2002 *Proc. 22nd Symp. on Fusion Technology (Helsinki, Finland)* p 1061

[32] Sihler C. *et al* 2003 *Proc. Int. Conf. on Power System Transients (New Orleans, USA)* http://www.ipst.org/IPST03Papers.htm (Generators and Machines, 6b-3)

[33] Ambrosino G., Ariola M., Pironti A. and Sartori F. 2003 *Fusion Eng. Des.* **66–68** 797

[34] Ariola M., De Tommasi G., Pironti A. and Sartori F. 2003 *Proc. 42nd IEEE Conf. on Decision and Control (Maui, Hawaii, USA)* p 4611

[35] Crisanti F. *et al* 2003 *Fusion Eng. Des.* **66-68** 803

[36] Albanese R., Calabro G., Mattei M. and Villone F. 2003 *Fusion Eng. Des.* **66–68** 715

[37] Villone F., Riccardo V., Albanese R., Sartori F. and Cenedese A. 2003 *Fusion Eng. Des.* **66–68** 709

[38] Solano E. *et al* 2003 *Proc. 30th EPS Conf. on Contr. Fusion and Plasma Physics (St Petersburg, Russia)* vol 27A (ECA) P1.106

[39] Arshad S. *et al* 1996 *23rd EPS Conf. on Controlled Fusion and Plasma Physics (Kiev, Ukraine)* vol 20C (ECA) P1-179

[40] Gauthier E. *et al* 1997 *24th EPS Conf. on Controlled Fusion and Plasma Physics (Berchtesgaden, Germany)* JET-P(97)12 (contributed paper)

[41] Coutlis A. *et al* 1999 *Nucl. Fusion* **39** 663

[42] Lister J.B. *et al* 2002 *Nucl. Fusion* **42** 708

[43] Cunningham G. *et al* 2002 *Proc. 29th EPS Conf. on Controlled Fusion and Plasma Physics (Montreux, Switzerland)* vol 26B (ECA) P5.092

[44] Hofmann F. *et al* 2000 *Nucl. Fusion* **40** 767

[45] Joffrin E. *et al* 2003 *Plasma Phys. Control. Fusion* **45** A367

[46] Moreau D. *et al* 2003 *Nucl. Fusion* **43** 870

[47] Gribov Y. *et al* 2000 *Proc. 18th Int. Conf. on Fusion Energy 2000 (Sorrento, 2000)* (Vienna: IAEA) CD-ROM ITERP/02 and http://www.iaea.org/programmes/ripc/physics/fec2000/html/node1.htm

[48] Gribov Y., Cavinato M., Kavin A., Khayrutdinov R., Lukash V. and Mondino P.L. 2001 *Proc. 28th EPS Conf. on Controlled Fusion and Plasma Physics (Funchal, Portugal)* vol 25A (ECA) p 617

[49] Shimada M. *et al* 2007 Progress in the ITER Physics Basis *Nucl. Fusion* **47** S1–S17

[50] ITER Physics Basis 1999 *Nucl. Fusion* **39** 2251

[51] Khayrutdinov R.R. and Lukash V.E. 1993 *J. Comput. Phys.* **107** 106

[52] Lukash V.,Gribov Y., Kavin A., Khayrutdinov R. and Cavinato M. 2005 *Plasma Devices Oper.* **13** 143

[53] Favez J.-Y., Lister J.B., Mullhaupt Ph., Srinivasan B. and Villone F. 2003 *Proc. 30th EPS Conf. on Controlled Fusion and Plasma Physics (St Petersburg, Russia)* vol 27A (ECA) P3.125

[54] Favez J.-Y., Lister J.B., Bonvin D., Muellhaupt Ph. and Srinivasan B. 2003 Enhancing tokamak control given power supply voltage saturation *Proc. 9th Int. Conf. on Accelerator and Large Experimental Physics Control Systems (Gyeongju, Korea)*

[55] Lister J.B. *et al* 2002 Plasma current, position and shape control *Lausanne Report* LRP 741/02 Contract FU05-CT2001-00018 (EFDA/00-551)

[56] Luce T.C. 2005 *Nucl. Fusion* **45** S86–97

[57] Joffrin E. *et al* 2005 *Nucl. Fusion* **45** 626

[58] Staebler A. *et al* 2005 *Nucl. Fusion* **45** 617

[59] Ongena J. et al 2004 *Nucl. Fusion* **44** 124

[60] Giannone L., Sips A.C.C., Kardaun O., Spreitler F., Suttrop W. and the ASDEX Upgrade Team 2004 *Plasma Phys. Control. Fusion* **46** 835

[61] Murari A. *et al* 2005 *Plasma Phys. Control. Fusion* **47** 395

[62] Ferron J.R. *et al* 2005 *Proc. of the 32nd EPS Plasma Physics Conference (Tarragona, Spain)* vol 29C (ECA) P1.069

[63] Casper T.A. *et al* 2006 *Plasma Phys. Control. Fusion* **48** A35

[64] Stober J. et al 2003 *Nucl. Fusion* **43** 1265

[65] Doyle E.J. *et al* 2007 Progress in the ITER Physics Basis *Nucl. Fusion* **47** S18–S127

[66] Loarte A. *et al* 2007 Progress in the ITER Physics Basis *Nucl. Fusion* **47** S203–S263

[67] De Esch H.P.L., Stork D., Challis C. and Tubbing B. 1995 *Fusion Eng. Des.* **26** 589

[68] Rebut P-H., Boucher D., Gambier D.J., Keen B.E. and Watkins M.L. 1993 *Fusion Eng. Des.* **22** 7

[69] Fukuda T. *et al* 1999 *Fusion Eng. Des.* **46** 337

[70] Lister J.B. 2000 *Nucl. Fusion* **40** 1167

[71] Equipe Tore Supra (prepared by F. Saint-Laurent) 2000 *Nucl. Fusion* **40** 1047

[72] Oikawa T. and the JT-60 Team 2000 *Nucl. Fusion* **40** 1125

[73] Allen S.L. and the DIII-D Team 2001 *Nucl. Fusion* **41** 1341

[74] Bosak K. *et al* 2003 *Proc. 30th EPS Conf. on Controlled Fusion and Plasma Physics (St Petersburg, Russia)* P3.164

[75] Tresset G. *et al* 2002 *Nucl. Fusion* **42** 520

[76] Felton R. *et al* 2000 *IEEE Trans. Nucl. Sci.* **47** 174

[77] Fukuda T. *et al* 2002 *Fusion Sci. Technol.* **42** 357

[78] Huysmans G.T.A. *et al* 1999 *Nucl. Fusion* **39** 1489

[79] Neyatani Y. *et al* 1997 *Fusion Eng. Des.* **36** 429

[80] Wijnands T. *et al* 1996 *Nucl. Fusion* **36** 1201

[81] Messian A. *et al* 1996 *Nucl. Fusion* **34** 39

[82] Tamai H. *et al* 1998 *Fusion Eng. Des.* **39** 163

[83] Dumortier P. *et al* 2003 *Proc. 30th EPS Conf. on Controlled Fusion and Plasma Physics (St Petersburg, Russia)* P1-91

[84] Jackson G.L. *et al* 1997 *J. Nucl. Mat.* **241–243** 618

[85] Ferron J.R. *et al* 2006 *Nucl. Fusion* **46** L13

[86] Gohil P. *et al* 2006 *Plasma Phys. Control. Fusion* **48** A45

[87] Mazon D. *et al* 2002 *Plasma Phys. Control Fusion* **44** 1087

[88] Laborde L. *et al* 2007 A model-based technique for real time control of current and pressure profiles in the JET tokamak *Eur. J. Control* submitted

[89] Tala T. *et al* 2004 *20th IAEA Fusion Energy Conf. (Vilamoura, Portugal)* TH-2.9

[90] Jardin S.C., Pomphery N. and Delucia J. 1986 *J. Comput. Phys.* **66** 481

[91] Khayrutdinov R.R., Lister J.B., Lukash V.E. and Wainwright J.P. 2001 *Plasma Phys. Control. Fusion* **43** 321

[92] Favez J.-Y., Khayrutdinov R.R., Lister J.B. and Lukash V.E. 2002 *Plasma Phys. Control. Fusion* **44** 171

[93] Raju D. *et al* 2002 *Proc. 29th EPS Conf. on Controlled Fusion and Plasma Physics (Montreux, Switzerland)* vol 26B (ECA) P2.082

[94] Leuer J.A. *et al* 1999 *Proc. 18th IEEE/NPSS Symp. Fusion Eng. (Albuquerque, New Mexico)* p 531

[95] Nakamura Y., Pautasso G., Gruber O. and Jardin S.C. 2002 *Plasma Phys. Control. Fusion* **44** 1471

[96] Nakamura Y. *et al* 2003 *Proc. 30th EPS Conf. on Controlled. Fusion and Plasma Physics (St Petersburg, Russia)* vol 27A (ECA) P2.128

[97] Fransson C.M., Edgell D.G., Humphreys D.A. and Walker M.L. 2003 *Phys. Plasmas* **10** 3961

[98] Humphreys D.A. *et al* 2003 *Proc. 20th Symp. on Fusion Engineering (San Diego, USA)* O1B-1